Spring 2009

Observations of Arctic haze from the NCAR C-130 during TOPSE(2000) and evidence of nitric acid uptake and redistribution by cirrus clouds during TC4(2007) obtained from the NASA DC-8

Eric M. Scheuer
University of New Hampshire, Durham

OBSERVATIONS OF ARCTIC HAZE FROM THE NCAR C-130 DURING TOPSE(2000) AND EVIDENCE OF HNO_3 UPTAKE AND REDISTRIBUTION BY CIRRUS CLOUDS DURING TC4(2007) OBTAINED FROM THE NASA DC-8

By

ERIC M. SCHEUER
Bachelor of Science, University of New Hampshire, 1993

THESIS

Submitted to the University of New Hampshire
in Partial Fulfillment of
the Requirements for the Degree of

Master of Science
in
Earth Sciences

May, 2009

This thesis has been examined and approved.

Robert Talbot

Thesis Director, Robert W. Talbot, Research Professor of Earth Sciences and Earth, Oceans and Space

Jack E. Dibb, Research Associate Professor of Earth Sciences and Earth, Oceans and Space

Barkley C. Sive, Research Associate Professor of Earth Sciences and Earth, Oceans and Space

April 9, 2009

Date

ACKNOWLEDGEMENTS

Funding for the TOPSE portion of this work was provided by the National Science foundation (NSF) Office of Polar Programs (OPP) through the National Center for Atmospheric Research (NCAR). Funding for the TC4 portion was provided by NASA through the Upper Atmospheric Research Program (UARP), Radiation Science Program (RSP) and Tropospheric Chemistry Program (TCP). I would like to thank Garry Seid for his help during the TOPSE field deployment and Cyndi Twohy, David Rogers, Andrew Heymsfield and Aaron Bansemer for access to data products relative to TC4. I would especially like to thank Robert Talbot and Jack Dibb for allowing me to participate in both projects and their subsequent support and guidance.

TABLE OF CONTENTS

LIST OF TABLES

LIST OF FIGURES

ABSTRACT

OBSERVATIONS OF ARCTIC HAZE FROM THE NCAR C-130 DURING TOPSE (2000) AND EVIDENCE OF HNO_3 UPTAKE AND REDISTRIBUTION BY CIRRUS CLOUDS DURING TC4 (2007) OBTAINED FROM THE NASA DC-8

By

Eric M. Scheuer

University of New Hampshire, May, 2008

The use of large aircraft is an invaluable tool for the study of chemical and physical processes in the atmosphere. In this thesis, some findings from two different major aircraft campaigns are reported. Part I examines measurements of fine aerosol sulfate in the Arctic made aboard the National Center for Atmospheric Research (NCAR) C-130 aircraft during the Tropospheric Ozone Production about the Spring Equinox Experiment (TOPSE) in 2000. Measurements highlighted the seasonal evolution of the Arctic haze phenomenon. Part II reports on measurements of nitric acid and various cloud microphysical properties made aboard the NASA DC-8 aircraft during Tropical Composition, Cloud, and Climate Coupling Experiment (TC4) in 2007. Results presented further our understanding of the role of tropical cirrus clouds in the redistribution of nitric acid which is an important component in upper tropospheric ozone production.

PART I

SEASONAL DISTRIBUTIONS OF FINE AEROSOL SULFATE IN THE NORTH AMERICAN ARCTIC BASIN DURING TOPSE

CHAPTER I

INTRODUCTION

Accumulation of aerosols and anthropogenic pollutant gases in the troposphere during the Arctic wintertime is well documented [*Rahn*, 1981, *Barrie*, 1986]. The slow transformation and removal processes because of cold sub-zero temperatures, absence of wet precipitation, and low levels of solar radiation [*Barrie*, 1986] coupled with low-level, long-range meridional transport of Eurasian mid and high latitudinal pollutants into the Arctic lead to annual wintertime events which have become to be known as Arctic haze. This visual haze is largely because of the aerosol light scattering properties of accumulation mode particles [*Brock et al.*, 1989], which exhibit a dominant presence around the 0.01-0.5 μm effective diameter range [*Blanchet and List*, 1983]. The hazes have been shown to be primarily of anthropogenic origin [*Radke and Hobbs*, 1984] with aerosol $SO_4^=$ constituting more than half of the total aerosol mass [*Shaw*, 1989]. Most of this $SO_4^=$ mass is derived from anthropogenic emissions of SO_2 rather than primary particulate emissions [*Barrie and Hoff*, 1984]. Much of these emissions are believed to have originated from Europe and Russia [*Rahn*, 1981] and been transported isentropically into the Arctic in multi-day long pulses as low pressure systems run up against the quasi-stationary Siberian high [*Barrie*, 1986].

Arctic Haze is believed to influence radiative budgets, snowpack albedo, snowpack chemical composition, and microphysical properties of Arctic clouds [*Brock et al.*, 1990]. Measurements of $SO_4^=$ aerosols in the Arctic have often been limited to

geographically fixed locations. These data tend to be lacking information on spatial variability, both horizontally and vertically. Intensive airborne measurement campaigns conducted in both the summer (ABLE 3A-3B, 1988, 1990) and winter (AGASP I-IV, 1983, 1986, 1989, and 1991) into the Arctic have reported only a limited number of aerosol $SO_4^=$ measurements because of relatively long sample integration times inherent to filter collection techniques.

In the early months of 2000, the heavily instrumented NSF/NCAR C-130 research aircraft conducted a series of trips into the Arctic beginning on February 4, 2000 and continuing until May 23, 2000. This campaign was called the Tropospheric Ozone Production about the Spring Equinox Experiment, or TOPSE. The primary objective of TOPSE was to study Arctic ozone production, loss and transport with a focus on the commonly observed springtime Arctic ozone maximum. It consisted of seven trips (42 total flights) from Boulder, Colorado (38°N) into the high Arctic environment (86°N). *Atlas et al.* [2003] provides an instrument payload description and detailed objectives of the flights conducted during TOPSE. A summary flight track plot including all flights conducted during TOPSE is shown as Figure I.1.

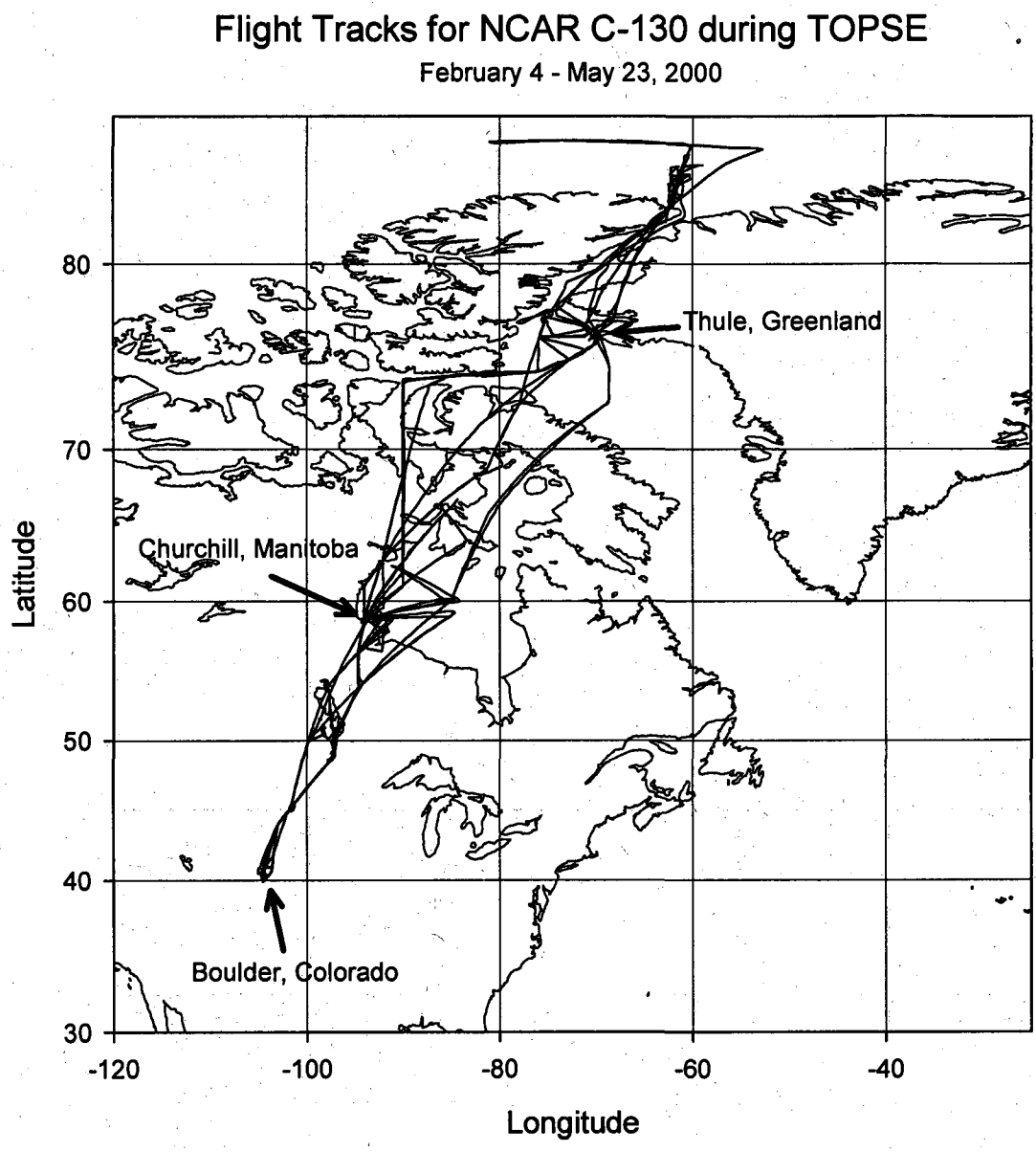

Figure I.1. TOPSE flight track summary Flight track summary for all 42 flights conducted during TOPSE.

This field campaign provided an excellent opportunity to use the University of New Hampshire's dual mist chamber/ion chromatograph technique to examine the seasonal and vertical distributions of fine aerosol $SO_4^=$ in the Arctic. This technique was developed for the measurement of soluble gases such as HNO_3, CH_3COOH, HCOOH

[*Talbot*, 1999], SO_2 [*Klemm and Talbot*, 1991], HCl [*Keene*, 1993], and HONO [*Dibb*, 2002b]. Experiments during prior intensive aircraft campaigns have demonstrated that with only minor modifications, measurements of fine soluble aerosols are possible. This technique is well suited for Arctic haze related aerosol $SO_4^=$ since the aerosols are present predominantly in the accumulation size mode [*Radke et. al.*, 1984]. Previously, soluble aerosol sampling has been restricted to Teflon filter exposure and subsequent solvent/water extraction. The Teflon filter technique, although yielding more potential analytes, suffers from long integration times, generally between 15 and 30 minutes. During the nearly 4-month period, 3820 samples were successfully collected using the mist chamber/ion chromatography technique with an average integrated collection time of 2.5 minutes. Analysis was performed in near-real time with detection limits as low as 4 parts per trillion by volume (pptv). To date, this was the most extensive $SO_4^=$ aerosol data set collected from an airborne platform.

Twenty bulk aerosol measurements were made during TOPSE using the NCAR-RAF Small Community Aerosol Inlet (SCAI) and Teflon filters. These measurements were made primarily to help speciate detectable, but unexpected, amounts of soluble Br^- detected by the mist chamber/ion chromatograph system in many low altitude samples. Aerosol $SO_4^=$ was also detected and quantified in these samples, providing some measure of comparison to the mist chamber samples.

CHAPTER II

METHODS

Sampling and Analysis

A schematic representation of the University of New Hampshire mist chamber/ion chromatograph is presented as Figure II.1.

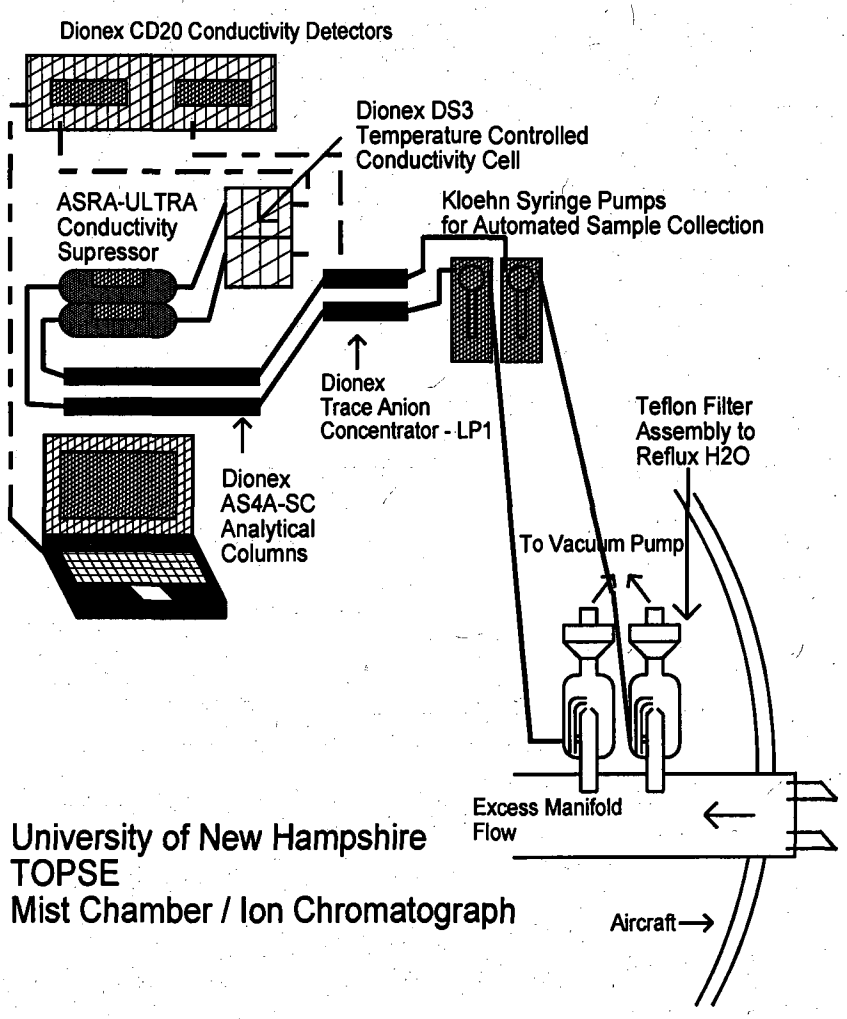

Figure II.1 Mist Chamber / Ion Chromatograph Schematic: Schematic diagram of the two-channel mist chamber/ion chromatograph used during TOPSE.

Soluble aerosols were collected in deionized water using two mist chambers operated alternately between a collection and analysis cycle similar to the system described by *Talbot et al.* [1999]. Operational descriptions of the mist chamber technique have been presented by *Cofer et al.* [1985], *Cofer et al.* [1986], *Talbot et al.* [1988], and *Talbot et al.* [1990]. Filters were not used on the sample inlet allowing aerosols to enter the sample stream. The mist chambers were connected to a sample manifold protruding from the aircraft about 25 centimeters, far enough to be in the free air stream and minimally affected by aircraft boundary layer effects. A 0.5-inch outer diameter inlet was positioned 90° to the airflow streamline over the aircraft, but was cut at a forward facing 45° angle. This 45° angle ensured that aerosol collected were small enough to make the 90° turn into the inlet, while larger particles were impacted on the inside face of the 45° cut. This design is believed to have excluded a majority of less radiatively important super-micron aerosols, commonly associated with sea salt and coarse mode dust. Based on particle stopping distance calculations eqn.5.3 and 5.19 in *Hinds* [1982], and an estimated average cruise speed of 129 meters per second (250 KTAS), the median cutoff particle size sampled by our inlet is estimated to be about 2.7 μm. Although this is a slightly larger cutoff than was desired, it still excludes a large percentage of coarse mode particles. Indeed, the bulk of the mass distribution of $SO_4^=$ in the Arctic has been shown to be accumulation mode aerosol $SO_4^=$, centered on 0.3 μm [*Blanchet*, 1989]. We believe that we sampled this size range effectively. A more rigorous inlet design and validation routine, although desirable, was not attempted because of time limitations, financial and airworthiness constraints coupled with the need to optimize passing of nitric acid (the species of primary interest to this instrument) in the same inlet.

Chemical analysis of the samples collected by the mist chambers was conducted in near real-time using ion chromatography. The aqueous samples were removed from the mist chamber by computer controlled syringe pumps (Kloehn 50300) and injected into custom fabricated ion chromatographs employing sample preconcentration (Dionex TAC-LP1). Separation was achieved using a helium purged carbonate/bicarbonate eluent and Dionex AS4A analytical columns. Background conductivity was suppressed using Dionex ASRS-Ultra suppressors. Detection of Cl^-, Br^-, NO_3^-, SO_3^- and $SO_4^=$ was accomplished using a Dionex CD20 conductivity detector equipped with a DS-3 temperature controlled cell. Sulfur dioxide is quickly converted in the mist chamber to aqueous sulfite (SO_3^-) which is easily detected by ion chromatography. Based on laboratory tests and sample stream filtering of $SO_4^=$, it has been determined that very little SO_3^- is converted to $SO_4^=$ in the very short time between sample collection and analysis. Digitized data was then sent to a data acquisition computer using standard ethernet communications where post processing took place. An internal spike of known aqueous concentration of phosphate into the mist chamber and subsequent analysis was used to track any evaporative losses of water from the mist chamber during sampling. Two independent systems operated in tandem, which allowed for continuous sampling with an average 2.5-minute time resolution. It is important to note that, unlike conventional filter techniques, all sample and fluid handling was in a closed system and isolated from the aircraft cabin ambient air to prevent contamination.

CHAPTER III

RESULTS

Filter Intercomparisons – Previous Missions

During the 1999 NASA aircraft campaign Pacific Exploratory Mission – Tropics B (PEM-Tropics B) in the South Pacific, we collected non-size selected aerosol $SO_4^=$ data using the standard Teflon filter technique and the mist chamber/ion-chromatography technique simultaneously. *Dibb et al.* [2002] describes the sampling methodology and presents some data for the samples collected using the Teflon filter technique. Filter exposure times averaged 14.2 minutes (σ=7.2) on the DC-8 and 14.8 minutes (σ= 5.4) on the P3-B. Because the standard Teflon filter technique was designed for bulk aerosol sampling rather than a size selected fraction, some correction to make the data comparable was necessary. Although most non-marine aerosol $SO_4^=$ mass is in accumulation size mode [*Warneck*, 1988], there can be a significant fraction associated with sea-salt or crustal dust that is in the much larger coarse mode, especially in a marine environment. This makes a simple sea-salt correction to the total $SO_4^=$ an acceptable method to approximate the fine aerosol $SO_4^=$ (or non-sea salt) component. Magnesium was used as the sea-salt tracer element for the determination of sea-salt $SO_4^=$. *Keene et al.* [1986] presents a discussion of the use of sea-salt ratios for the determination of sea-salt and non sea-salt components of marine aerosols. Examples from the PEM-Tropics B experiment conducted in the South Pacific of the comparison between fine aerosol $SO_4^=$

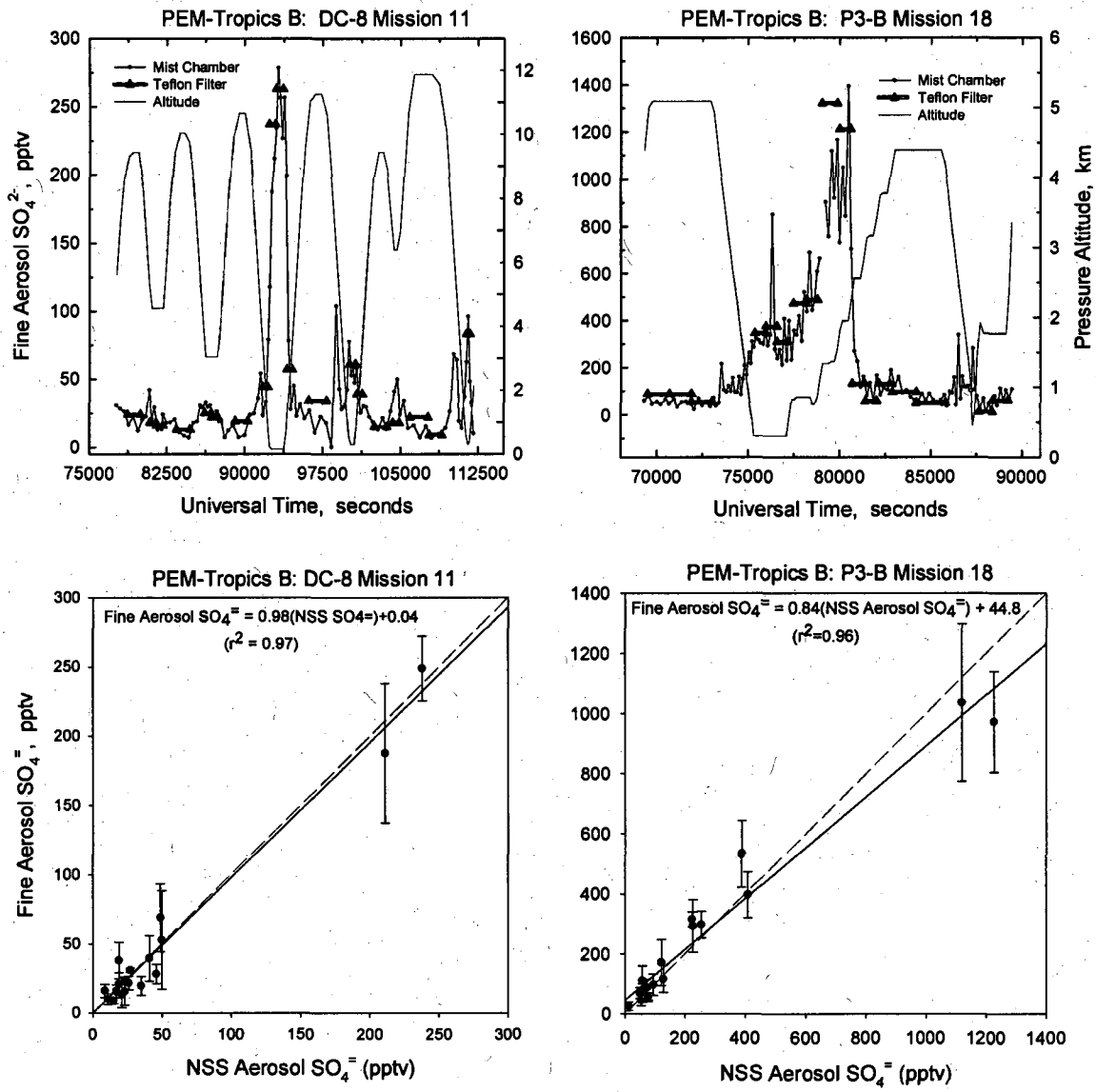

Figure III.1 Comparison of Mist Chamber to Filter Data–PEM-TROPICS B: Example intercomparisions of non-sea-salt $SO_4^{=}$ mixing ratios from filter samples and fine aerosol $SO_4^{=}$ from the mist chamber technique on different aircraft during PEM-Tropics B. In the top panel time-series plots, the length of the horizontal bars reflects filter exposure intervals. Mist chamber derived values are plotted at sample mid-point. The lower panels are scatter plots with least-squares regressions. For comparison, the dashed line is a 1:1 slope. Mixing ratios determined by the mist chamber technique (vertical axis) are averaged over the collection period of each filter (horizontal axis). Vertical error bars represent 1 standard deviation of mist chamber mixing ratios.

(mist chamber/ion chromatograph) and non-sea salt $SO_4^=$ (Teflon filters) from both the NASA DC-8 and the NASA P3-B research aircraft are presented in Figure III.1. Visual inspections of the data sets from each technique suggest that they are comparable. The mist chamber/ion chromatography technique exhibits much better time resolution than the Teflon Filter technique. This can be especially important during aircraft ascents and descents where a discrete sample represents a non-uniform altitude. Minimizing sample integration times becomes important in minimizing the vertical extent over which a sample is integrated. Filter samples are often not collected during ascents and descents because of this non-uniform altitude averaging issue.

Filter Intercomparisons during TOPSE

The NCAR Small Community Aerosol Inlet (SCAI) with flow straightening shroud and a University of New Hampshire modified curved leading edge nozzle was employed during TOPSE to sample the aerosol associated radionuclide tracers ^7Be and ^{210}Pb [*Dibb*, 2003]. This inlet was also used to collect a limited number of bulk aerosol samples isokinetically on Teflon filters at low altitudes (<2 km asl). These samples were collected in order to facilitate speciation of soluble bromide observed in the mist chamber/ion chromatography analysis, however, aerosol $SO_4^=$ was also quantified in these samples. This provided a basis for comparison of TOPSE mist chamber/ion chromatography samples to bulk aerosol filer samples. Figure III.2 shows that when $SO_4^=$ is measured using the two techniques, the data appear comparable. The variability in the mist chamber data represents the standard deviation of the mean mixing ratio measured by the mist chamber during the approximately 15 minute time period that a bulk filter

sample was being collected. It is not unexpected that the bulk aerosol data has a tendency to show slightly higher mixing ratios than the mist chamber data this close to the surface. Intercomparisons during the NASA PEM-Tropics B experiment suggest that agreement is even better at higher altitudes where $SO_4^=$ is almost exclusively on fine aerosols and uninfluenced by sea-salt or crustal dust.

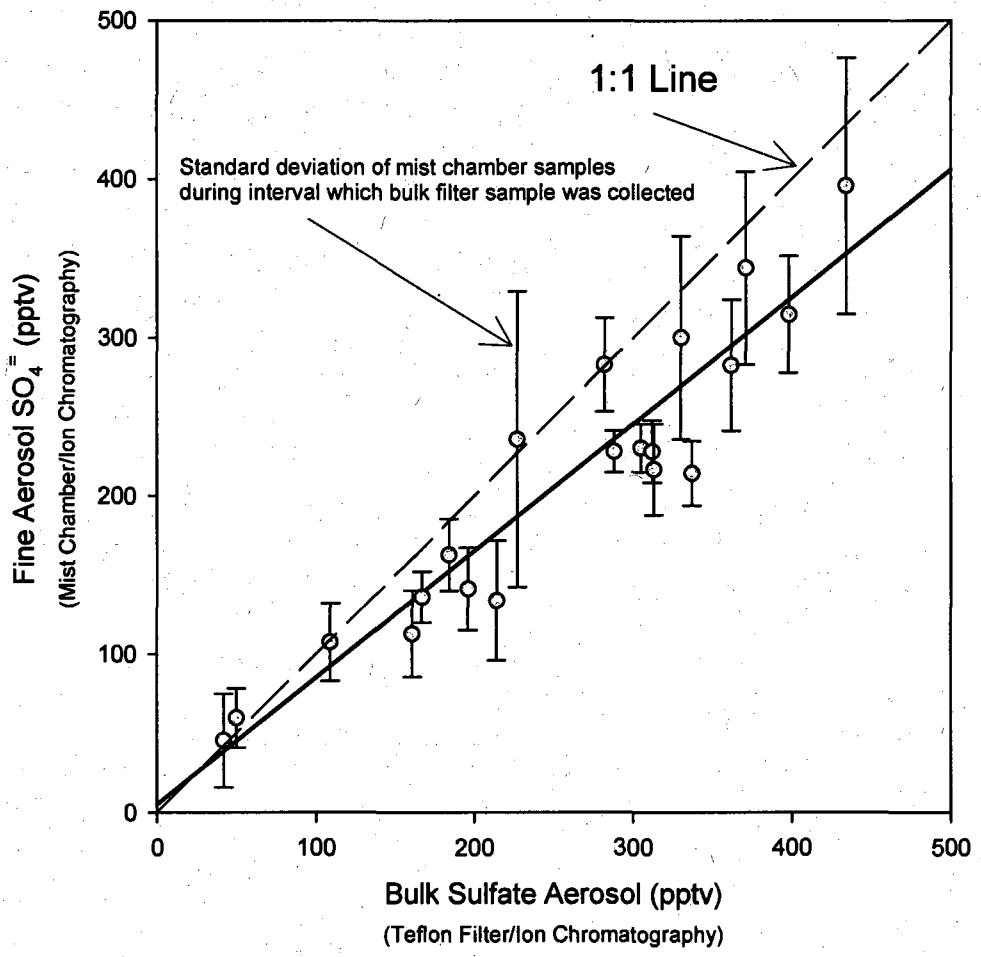

Figure III.2 Comparison of Mist Chamber to Filter Data–TOPSE: Intercomparision of the mist chamber/ion chromatograph technique to Teflon filter bulk aerosol $SO_4^=$ samples from TOPSE during periods of collection of the bulk aerosol samples. There were an average of 6 mist chamber samples collected for each of the approximately 15 minute bulk filter sample.

Fine Aerosol $SO_4^=$ Measured during TOPSE

A summary of the fine aerosol $SO_4^=$ data collected during TOPSE is presented in Table III.1. Data in the table represents samples collected at latitudes greater than 50°N, since data collected south of 50°N were generally collected during transit flights to the primary study region. In order to examine the seasonal evolution of fine aerosol $SO_4^=$ in the Arctic, the data were summarized by trip and grouped into discrete 1000-meter altitude bins in the latitude range of 50°N-86°N. Mixing ratios as high as 1766 pptv and as low as 4 pptv were observed during TOPSE (Table 1). The lowest values were generally observed during the first trip in early February. This trip also had the lowest variability in most altitude bins. The highest values were observed during the sixth trip in late April, which also exhibited the greatest variability.

Table III.1 Summary of Fine Aerosol Collected during TOPSE: Data presented were all collected north of 50° latitude and binned by trip and altitude. Mixing ratios are presented as geometric means. The geometric mean (M) commonly used for log-normally distributed data. It is the n^{th} root of the product of the values in a given bin. [$M_{(x)} = (x_1 x_2 \ldots x_n)^{1/n}$].

		Sample Count	Median (pptv)	Geometric Mean (pptv)	Minimum (pptv)	Maximum (pptv)
Trip 1				*February 4-9 (Flights 5-8)*		
	<1000 meters	31	124	112	28	290
	1000-2000 meters	11	51	54	20	130
	2000-3000 meters	21	58	61	18	188
	3000-4000 meters	21	43	47	20	124
	4000-5000 meters	17	43	41	16	131
	5000-6000 meters	69	23	25	6	235
	6000-7000 meters	10	23	19	12	25
	>7000 meters	2	32	31	25	39
Trip 2				*February 21-27 (Flights 9-13)*		
	<1000 meters	59	165	155	48	406
	1000-2000 meters	52	99	97	23	1766
	2000-3000 meters	39	53	51	16	126
	3000-4000 meters	29	59	49	12	132
	4000-5000 meters	40	69	57	14	140
	5000-6000 meters	113	50	50	18	150
	6000-7000 meters	20	45	50	22	313
	>7000 meters	28	39	44	21	103
Trip 3				*March 5-8 (Flights 14-17)*		
	<1000 meters	34	171	168	98	313
	1000-2000 meters	14	117	142	44	552
	2000-3000 meters	24	133	105	4	530
	3000-4000 meters	13	117	83	8	543
	4000-5000 meters	21	86	101	23	337
	5000-6000 meters	35	50	46	8	189
	6000-7000 meters	37	27	30	9	214
	>7000 meters	15	43	37	12	117
Trip 4				*March 19-26 (Flights 18-23)*		
	<1000 meters	85	206	225	116	667
	1000-2000 meters	58	242	219	19	540
	2000-3000 meters	69	211	158	40	597
	3000-4000 meters	40	133	129	34	446
	4000-5000 meters	76	130	125	33	498
	5000-6000 meters	110	126	109	47	473
	6000-7000 meters	40	104	109	46	242
	>7000 meters	51	116	118	49	268
Trip 5				*April 2-7 (Flights 24-30)*		
	<1000 meters	85	219	209	95	598
	1000-2000 meters	43	212	217	76	504
	2000-3000 meters	33	243	221	85	400
	3000-4000 meters	33	200	194	87	364
	4000-5000 meters	93	183	176	73	407
	5000-6000 meters	110	129	122	43	324
	6000-7000 meters	79	122	120	63	307
	>7000 meters	26	131	136	59	313
Trip 6				*April 23-30 (Flights 31-36)*		
	<1000 meters	97	223	184	26	628
	1000-2000 meters	48	189	208	78	597
	2000-3000 meters	68	236	237	84	784
	3000-4000 meters	40	191	171	33	842
	4000-5000 meters	65	199	173	4	684
	5000-6000 meters	168	157	140	57	1160
	6000-7000 meters	25	172	199	69	698
	>7000 meters	59	110	120	21	470
Trip 7				*May 15-23 (Flights 37-42)*		
	<1000 meters	70	173	149	21	322
	1000-2000 meters	64	170	162	20	722
	2000-3000 meters	45	187	143	10	788
	3000-4000 meters	62	170	153	27	374
	4000-5000 meters	61	175	157	36	417
	5000-6000 meters	179	171	160	32	487
	6000-7000 meters	58	128	124	30	390
	>7000 meters	24	162	143	59	400

Our measured values are consistent with data presented in *Lazrus and Ferek* (1984) from the 1983 AGASP airborne sampling campaign. They report $SO_4^=$ concentrations in the Arctic as low as 7.3 neq/m^3 (82 pptv) and as high as 110 neq/m^3 (1233 pptv). However, their data represent samples collected over much longer periods of integration, and are less likely to represent a completely homogenous sample. This explains the smaller range of mixing ratios reported. Their highest value presented is reported to have been collected while flying in a continuous haze layer and may reflect a more homogeneous sample. Indeed, their highest mixing ratio reported is very similar to what we observed.

The frequency distribution of our raw aerosol $SO_4^=$ data is highly skewed by less frequent but very high values. This can be explained by an abundance of cleaner air riddled with thin, highly polluted, layers. That is, because the polluted layers can be strongly delineated from the cleaner air, there appeared to be an absence of more moderate transition layers. Arithmetic means are only representative of data that has an approximately normal frequency distribution. This makes using arithmetic means for our $SO_4^=$ data bins very misleading. Using medians can have the opposite effect since the median is not very sensitive to our less frequently occurring, but very large observations. To address this problem, we use geometric means. This statistic can be applied since the data are more nearly log-normally distributed. This statistical tool addresses more of the real variability within the data set without placing emphasis on unusually high or low values. It also allows us to visualize real variability in the form of log-normally transformed standard deviations; presented graphically as unequal length error bars in Figure III.3.

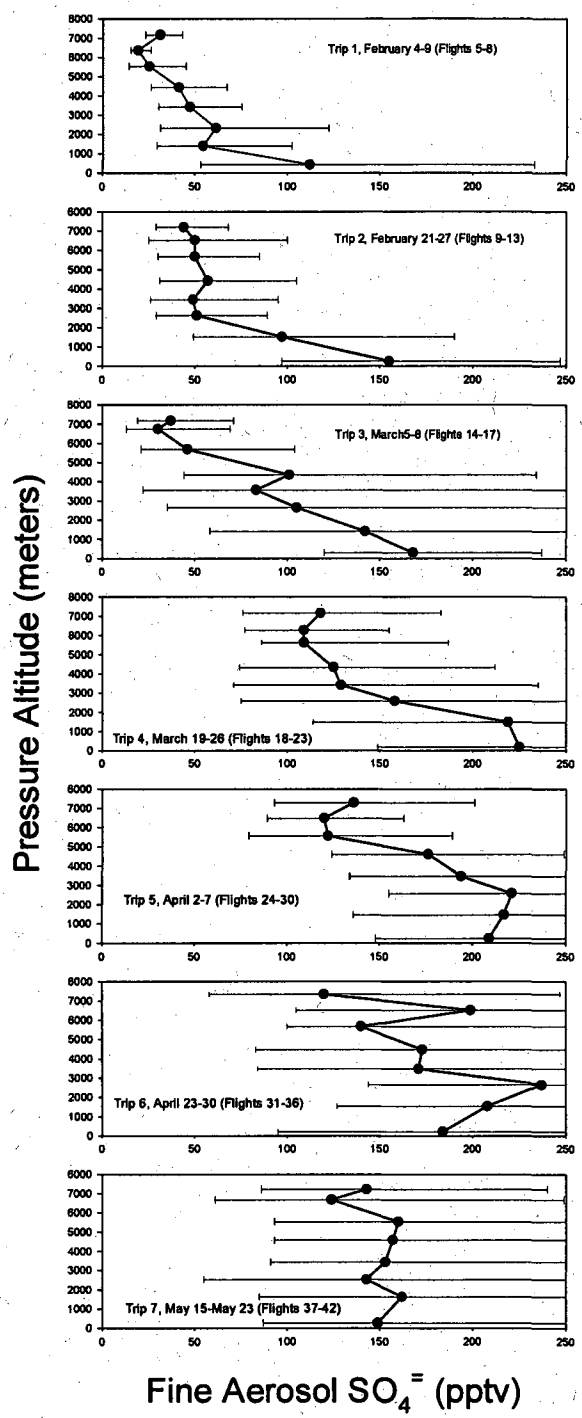

Figure III.3 Fine Aerosol $SO_4^=$ Vertical Distribution: Vertical distributions of geometric mean mixing ratios between 50 and 85 north latitude. Error bars represent 1 standard deviation about the geometric mean and are asymmetric. They represent a measure of variability of mixing ratios observed (about 68%) and not error.

During the first trip in early February, fine aerosol $SO_4^=$ mixing ratios were relatively low and not highly variable above 1000 meters (Figure III.3, top panel). Below 1000 meters the range of mixing ratios was significantly higher and yielded a geometric mean of 110 pptv. This mean was more than two-fold higher than in any other altitude bin during this trip. Interestingly, *Ridley et al.* (2003) report a rarity of pollution events at very low altitude. $SO_4^=$ mixing ratios were, however, noticeably enhanced all the way to the lowest altitudes surveyed during TOPSE throughout the campaign. *Barrie* (1986) reported data summarized in *Rahn and Heidman* (1981) noting that winter/spring pollution aerosols measured from a ground based Arctic aerosol sampling network averaged 2 $\mu g/m^3$ $SO_4^=$ (466 pptv). This is consistent with our observations of near-surface $SO_4^=$ enhancements.

During the second trip (late February), mean mixing ratios in the two lowest bins were almost double what was observed during the first trip, but mean mixing ratios above 2000 meters remained around 50 pptv and were not highly variable. This trend of increasing mean mixing ratios at increasingly higher altitudes as the season progresses continued into trip 3 in early March. Mean mixing ratios below 5000 meters all appeared to be enhanced and increasingly variable with respect to earlier trips. There was also a gradient of about 70 pptv in mean mixing ratios (100 to 170 pptv) between the 2000 to 3000 meter bin and below 1000 meters.

Mean mixing ratios were above 100 pptv in all altitude bins and above about 225 pptv below 2000 meters by trip 4 in late March. The steepest gradient in $SO_4^=$ mean mixing ratio was no longer below 1000 meters, but rather between 1000 and 3000 meters. The trend of increasing mean mixing ratios in all altitude bins from trip to trip but

decreasing mean mixing ratios with altitude began to show marked change during trip 5 in early April. Mean mixing ratios below 2000 meters were lower than on the previous trip while mean mixing ratios above 2000 meters continued to increase, albeit less dramatically. During the last two trips, fine aerosol sulfate mean mixing ratios generally continued to decrease below 3000 meters and increase above 4000 meters. By the end of the data collection phase of TOPSE, $SO_4^=$ mean mixing ratios showed no obvious altitude gradient and were greater than 3-fold higher at all altitudes above 1000 meters than they were in early February (about 30 percent higher below 1000 meters).

Talbot et al. [1992] reported aerosol sulfate mixing ratios averaging 29 pptv in the boundary layer and 65 pptv in the free troposphere during the ABLE 3A (1988) summer campaign in the Arctic. This suggests that $SO_4^=$ mixing ratios in the high Arctic should continue declining through late spring into the summer, possibly exhibiting a gradient inverse to that noted in the earlier TOPSE trips. This decrease must happen rapidly during the month of June, and is likely related to the onset of warmer temperatures and liquid precipitation.

The seasonal evolution of aerosol $SO_4^=$ in the Arctic is shown in a different format in Figure III.4. Mean mixing ratios of $SO_4^=$ below 2000 meters increased during early February until the end of March, reaching a mean mixing ratio maximum of about 220 pptv. Mean mixing ratios declined to about 150 pptv during April and May. In the middle troposphere (2000-5000 meters), mixing ratios continued to increase until the end of March, reaching a mean mixing ratio peak of 200 pptv. In the upper Arctic troposphere, mean mixing ratios appeared to still be increasing at the conclusion of the sampling campaign, but had not exceeded levels in the lower and middle troposphere

(which were already declining from peak values). The sharp decreasing trends in mean mixing ratios in the lower and middle troposphere coupled with the still increasing or flat gradients in the upper troposphere would produce the summertime inverse gradient observed by *Talbot et al.* [1992].

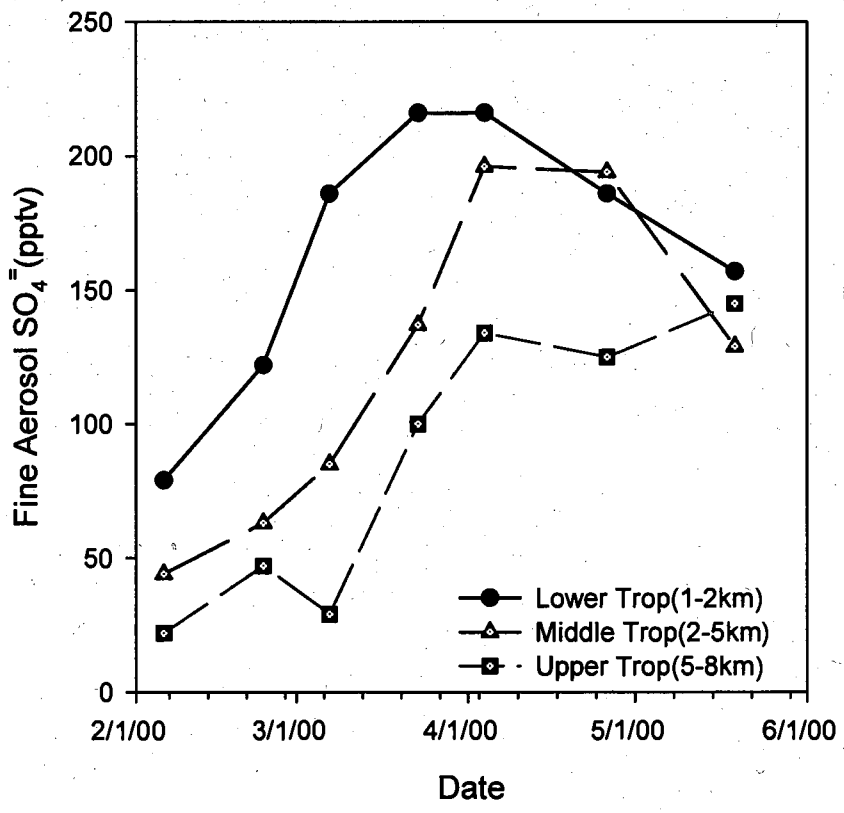

Figure III.4 Seasonal Progression of Fine Aerosol $SO_4^=$: Seasonal progression of geometric mean mixing ratios of fine aerosol $SO_4^=$ in three altitude bins.

To examine latitudinal trends in aerosol $SO_4^=$ data collected during TOPSE, we binned data into two seasons (winter and spring) and three altitude bins (below 2000 meters, 2000-5000 meters, and above 5000 meters). All values measured north of 50°N

were plotted along with binned 5° latitude geometric means (Figure III.5) to demonstrate the variability that characterized the Arctic troposphere.

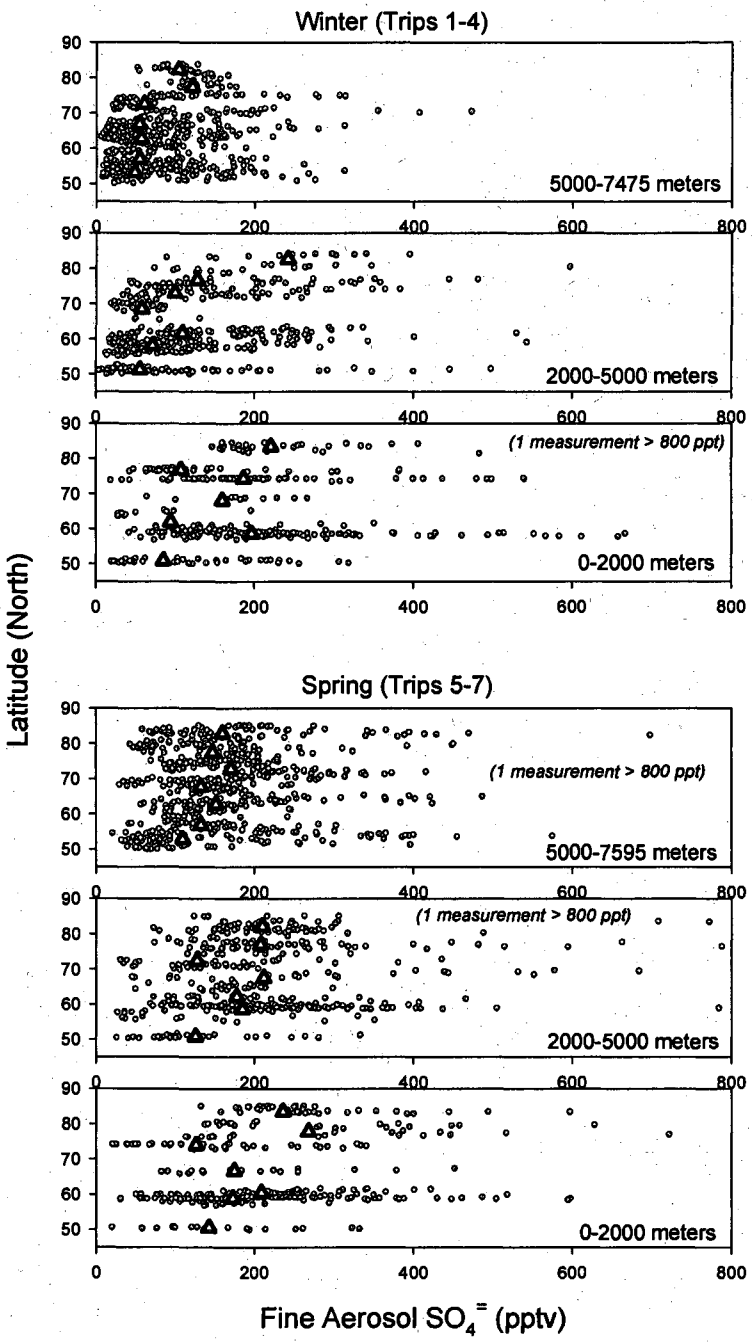

Figure III.5 Latitudinal Distributions of Fine Aerosol $SO_4^=$: Latitudinal distributions of fine aerosol $SO_4^=$ during winter and spring in 3 altitude bins. Raw data shown (circles) are discrete measurements made north of 50°N. Triangles represent geometric means of $SO_4^=$ mixing ratios plotted at the mean latitude of the 5° bins.

This extreme variability results from samples that were collected both in and out of haze layers. Mean mixing ratios appear to increase with latitude at all altitudes in both winter and spring, but only minimally. There is a more notably sharp gradient in minimum values measured north of about 70°N. This is especially evident in the lower troposphere in both the spring and winter. This trend in elevated minimum mixing ratios is also seen at higher altitudes, but the gradient is less steep. However, it does continue to lower latitudes. This is consistent with, and a nice illustration of, the 7-8 kilometer deep "polar dome" described in *Barrie* [1986] and *Shaw and Khalil* [1989].

CHAPTER IV

DISCUSSION

The seasonal trend in vertical aerosol $SO_4^=$ distribution during TOPSE is clear in Figure III.4. During early February, significant enhancements in aerosol $SO_4^=$ appear to be strongly confined near the surface. Long-range transport from the northern Eurasian continent along low level, sinking isentropes is likely most responsible for this observation. As the season progresses from winter to spring, this phenomenon of long-range isentropic transport begins to ascend vertically. Evidence that the polluted parcels of air are confined to near the surface disappears as dramatically enhanced mixing ratios are observed at higher altitudes. We believe that, even in the late winter, vertical mixing is a small or non-existent component of the observed enhancement at higher elevations. Mixing of low-level air with the overlying free troposphere is inhibited by a persistent low-level inversion [*Kahl*, 1990]. Stable inversions can last for several weeks essentially decoupling the lower troposphere from higher altitudes [*Bradley et al.*, 1992]. Elevated mixing ratios at higher and higher altitudes as the season progresses must be explained by transport into the Arctic along vertically higher isentropes tracing back to warmer and warmer source regions in northern Eurasia. A discussion of isentropic transport pathways coupled with source region potential temperatures during TOPSE is presented by *Klonecki* et al. [2003].

During early April, below 3000 meters, levels of $SO_4^=$ enhancement began to decline. An increase in inversion base depths and decrease in inversion persistence probabilities [*Kahl et al.*, 1992] hint that solar surface heating may be beginning to stir up the lowest levels of the atmosphere while more stable isentropic transport can continue at higher altitudes. Removal processes, dominated by wet deposition [*Barrie*, 1985], become increasingly important and decrease mixing ratios at lower altitudes. By the end of May, surface mixing ratios of fine aerosol $SO_4^=$ are almost half of the maximum observed in March. Mixing ratios also appear to be beginning to decrease at higher altitudes. This is consistent with the much lower values observed at all altitudes during summer months by *Talbot et al.* [1992].

The high variability observed in Figure III.5 demonstrate that $SO_4^=$ aerosol mixing ratios in the Arctic winter are far from homogeneous. Mixing ratios during the late February trip (trip 2) in the 1000-2000 meter altitude bin were observed to be as low as 23 pptv and as high as 1766. This is consistent with prior observations of multiple narrow haze bands covering between 20-200 kilometers [*Radke et. al.*, 1984] which are often between tens of meters to 1 kilometer thick, [*Brock et al.*, 1989] and streaming slowly into the Arctic environment. Individual altitude bins of data presented here probably incorporate both cleaner and more polluted layers, leading to high variability within the bins. The observations of increasing $SO_4^=$ mean mixing ratios in an altitude bin during the winter can be attributed to more frequent occurrences of these narrow polluted layers within the bin region.

CHAPTER V

CONCLUSIONS

The mist chamber/ion chromatograph is shown to be an effective tool for the measurement of fine aerosol $SO_4^=$ aboard an aircraft platform. During TOPSE, we collected an extensive fine aerosol $SO_4^=$ data set. These measurements paint a four month long picture of the vertical distributions in the Arctic. Small-scale variability and poorly understood frequencies of haze layers, however, makes estimation of total aerosol burdens difficult [*Brock et al.*, 1990]. The slow transport and lack of major chemical transformations allow us to treat the approximately weeklong measurement campaigns as synoptic snapshots of the Arctic environment. It is shown that $SO_4^=$ aerosols begin to build up at very low altitudes during the winter. The altitude at which the buildup is most pronounced tended to migrate to higher altitudes as the season progressed toward spring. In spring, $SO_4^=$ aerosols began to clean up at lower altitudes first, progressing upward. It is possible that much of the fine detail of the Arctic air is lost in the averaging and temporal gaps in the data. Follow-up investigations into the frequency, distribution, and spatial variability of Arctic pollution layers could help provide better information into the extent and magnitude of these layers as well as help better explain the extreme heterogeneity observed.

PART II

EVIDENCE OF NITRIC ACID UPTAKE IN WARM CIRRUS CLOUDS DURING THE NASA TC4 CAMPAIGN

CHAPTER VI

INTRODUCTION

Gas phase nitric acid (HNO_3) is a primary reservoir species of atmospheric nitrogen oxides (NO_x = NO+NO_2) [*Neuman et al.*, 2001; *Staudt et al.*, 2003] which play an important role in upper tropospheric (UT) ozone production [*Jacob et al. 1996*]. Many past global chemistry models have over predicted UT HNO_3 by factors ranging from two to ten [*Thakur et al.*, 1999] suggesting that removal mechanism were poorly understood. *Lawrence and Crutzen* [1998] suggested that efficient removal of HNO_3 by adsorptive uptake onto cirrus cloud ice particles and subsequent gravitational sedimentation had the potential to significantly redistribute or remove HNO_3 in the UT, explaining some of the discrepancies between measurements and models. Initial laboratory investigations into HNO_3 uptake onto ice surfaces found that the process is efficient, and appears to proceed until there is a high fractional surface coverage of available adsorption sites. However, details of the uptake have varied between experiments using ice particles and films, which may be less than ideal surrogates for crystals in cirrus clouds. Also, most of the experiments used initial HNO_3 partial pressures greatly in excess of those likely in the UT, requiring large and poorly constrained extrapolations to relevant vapor pressures [*Abbat*, 1997; *Zondlo et al.*, 1997; *Arora et al.*, 1999; *Hudson et al.*, 1999; *Hynes et al.*, 2002]. *Tabazadeh et al.* [1999] assessed the results of several lab studies and presented a Langmuir surface chemical model that assumed the isotherm was dissociative and concluded that uptake of HNO_3 onto cirrus may be nearly an order of magnitude less

efficient than *Lawrence and Crutzen* [1998] assumed. *Tabazadeh et al.* [1999] also suggested that sublimation of cirrus crystals within several kilometers below clouds would limit the extent of vertical redistribution of HNO_3 by this process. A box model employed by *Meier and Hendricks* [2002] expands on assumption from *Tabazadeh et al.* [1999] for a much wider range of ambient conditions and sedimentation efficiencies and suggests under some conditions that HNO_3 uptake on cirrus ice and gravitational sedimentation could still be an efficient denitrification mechanism. Laboratory studies reported in *Ullerstam et al.* [2005] were the first to be performed at HNO_3 partial pressures more typical of the UT and confirmed some aspects of prior studies. HNO_3 uptake on ice surfaces in these experiments was found to be positively correlated with overlying HNO_3 partial pressures at low vapor pressures and available ice surface area, and negatively correlated with temperature. However, surface coverage was found to be far from saturation at partial pressures of HNO_3 typical of the UT, and uptake followed conventional non-dissociative Langmuir isotherm. *Ullerstam et al.* [2005] also noted that conventional and non-dissociative Langmuir treatments of HNO_3 uptake on ice predict similar behavior at high vapor pressures but diverged markedly at low pressures.

The first in situ aircraft measurements to provide evidence for uptake of HNO_3 by cirrus ice were reported in *Weinheimer et al.* [1998]. They measured the sum of condensed plus gas phase reactive nitrogen (NO_y) through a forward facing inlet compared to a gas phase only rear facing inlet to infer that up to 20% of NO_y was adsorbed onto ice in a mountain wave cloud over Colorado. Nitric acid was assumed to be the only component of NO_y taken up by ice. Surface coverages on the cirrus crystals were later estimated to be in the range of 1-4 x 10^{13} molecules cm^{-2} for measurements

made near the tropopause at ~215 K [*Hudson et al.*, 2002]. Several subsequent aircraft studies have also used similar dual inlet equipped NO_y instruments to estimate HNO_3 on ice crystals in the upper troposphere. *Melinger et al.* [1999] estimated coverages of 1 x 10^{13} molecules cm^{-2} in Arctic cirrus at ~196K, much lower than estimates near 2 x 10^{14} molecules cm^{-2} reported in *Kondo et al.* [2003] in Arctic clouds at temperatures ~210 K. Extensive measurements at midlatitudes reported in *Ziereis et al.* [2004] indicate coverages in the range 1 - 10 x 10^{13} and 0.5 - 1.5 x10^{13} molecules cm^{-2} at 214 K and 227 K, respectively. In both cases the inferred vapor pressure of HNO_3 corresponding to the high end of the estimated molecular coverage range was greater than a factor of four higher than estimates for the low end of the range. Direct measurements of condensed and gas phase HNO_3 in subtropical cirrus during the NASA CRYSTAL-FACE campaign are presented in *Popp et al.* [2004]. These data were also obtained with a similar dual inlet arrangement, but HNO_3 was quantified directly by chemical ionization mass spectrometry (CIMS) rather than inferred from NO_y measurements. Mean surface coverages of 6 x 10^{13} molecules cm^{-2} at 198 K and about 2 x 10^{13} molecules cm^{-2} at 200 K - 220 K were estimated. *Popp et al.* [2004] suggested that the samples at temperatures below 200 K were impacted by nitric acid trihydrate (NAT), thus not truly comparable to cirrus ice and point out that the rest of their observations indicate very weak, or no, dependence on temperature. *Ullerstam et al.* [2004] compared the results of these different field studies and suggested that overall the studies on thin ice films in flow tubes were qualitatively consistent and concluded that HNO_3 uptake in real clouds should generally increase at higher HNO_3 vapor pressures and at lower temperatures (although the *Melinger et al.* [1999] results do not fit this generalization with very low estimated

surface coverages at cold temperatures). However, they also noted that when a conventional non-dissociative Langmuir isotherm model fitted to their laboratory results was used to estimate surface coverages at the conditions of the various field studies, observed values were generally smaller than the estimates.

In this portion of the thesis, we report the first field evidence for uptake of HNO_3 onto tropical cirrus crystals in the intertropical convergence zone (ITCZ) near Costa Rica using measurements of gas phase HNO_3, ice water content (IWC), and surface area density (SAD). These observations extend the temperature range of in situ studies nearly to 245 K and explore quite low HNO_3 vapor pressures. Simultaneous measurements of condensed phase HNO_3 are not available, adding uncertainty to our quantitative estimates of HNO_3 surface coverage on ice, but we suggest the estimates are still informative beacuse they are based on observations in quite warm cirrus several kilometers below the tropopause.

CHAPTER VII

METHODS

TC4 Mission

NASA's Tropical Composition, Cloud and Climate Coupling (TC4) experiment in July and August, 2007 deployed the DC-8, ER-2 and WB-57 aircraft to Costa Rica to study deep convection in the ITCZ and its impact on the tropical tropopause layer (TTL). The primary role of the DC-8 was to characterize the chemical and microphysical properties of the troposphere to constrain the composition of air being entrained into the convection. However, much of the convective outflow and resulting cirrus near Costa Rica during the campaign was close to the 13 km ceiling of the DC-8. As a result, roughly half of all DC-8 sampling time targeted the upper troposphere (9-13 km) and most of that time was in and near cirrus clouds. Here we report on observations of in situ HNO_3, IWC, and SAD during three flights that targeted cirrus shields from specific convective cores to examine the extent of depletion of gas phase HNO_3 by uptake on ice crystals in these clouds.

HNO_3 Measurements

Gas phase HNO_3 was measured with the University of New Hampshire automated dual mist chamber/ion chromatograph system (MC/IC). In this system, ambient air is drawn into the aircraft at high velocity through a short (<1 meter), Silcosteel® (Restek, Inc., Bellefonte, PA) coated manifold at approximately 3 m^3 (volumetric) min^{-1}. Ambient

air is sub-sampled nominally at approximately 45-50 L min^{-1} (volumetric) by one of a pair of glass mist chambers mounted on the high flow manifold. The mist chamber inlets are rear facing with respect to the flow in the manifold, effectively excluding particles greater than about 1 μm. Discrete samples integrated for approximately 85 seconds are alternately collected by each mist chamber. While one mist chamber is sampling, the preceding sample collected in the other mist chamber is injected into an ion chromatograph where HNO_3 is detected as the nitrate (NO_3^-) ion. HNO_3 detection limits varied inversely with the mist chamber mass flow rate which decreases with altitude, but were typically better than 3 parts per trillion by volume (pptv). Variants of this instrument have been flown on the DC-8 during more than 10 prior campaigns (TRACE-A, PEM-WEST A and B, PEM-TROPICS A and B, SONEX, PAVE, TRACE-P, INTEX A and B) and is similar to that described Chapter II.

Ice Water Content Measurements

Cloud water content (CWC) in cirrus cloud was measured using the NCAR counterflow virtual impactor (CVI) as described in *Twohy et al.* [1997]. It is assumed that for all measurements presented here, all CWC is cirrus ice, or IWC. Ice crystals with aerodynamic diameters greater than 8 microns are separated from interstitial air using dry nitrogen counter flow at the inlet tip of the forward facing inlet. A hygrometer is used to measure water content of the evaporated ice crystals that enter the inlet.

Ice Surface Area Density Measurements

Estimates of geometric SAD of cloud ice particles were derived using data obtained from a Droplet Measurement Technology (DMT) Cloud Imaging Probe (CIP) and Precipitation Imaging Probe (PIP). The CIP and PIP probes provide two dimensional images of cloud ice particles. Equations provided in *Schmitt and Heymsfield* [2005] are used to estimate surface area of the three dimensional ice particles from the two dimensional images.

All data and analyses presented here are temporally merged where the IWC and SAD observations are averaged over the integration time of each mist chamber sample. All original data is available from the NASA Earth Science Project Office (ESPO) archive.

CHAPTER VIII

RESULTS

We focus on three flights conducted on July 31, August 5, and August 8, 2007. During these flights extended periods of time were spent flying in orbital "racetrack" patterns within cirrus clouds (Figure VIII.1).

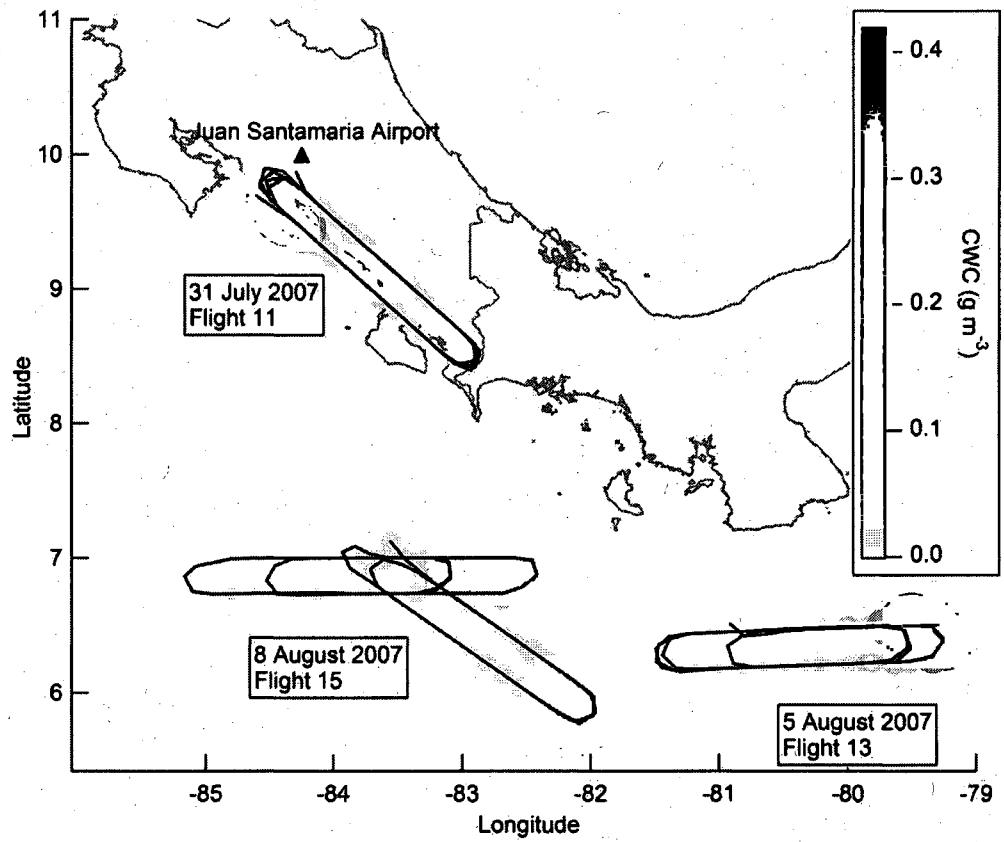

Figure VIII.1 Flight Track Map of TC4 Study Area: Map of racetrack maneuvers during TC4 flights on July 31, August 5 and August 8. Circles represent measurements of condensed water content in $g \cdot m^{-3}$ averaged to the HNO_3 measurement integration time and show progression of aircraft in and out of heavy cirrus cloud.

The purpose of the racetracks was to observe the evolution of cloud microphysical characteristics as measured by a number of in situ sensors on the DC-8 and by remote sensors deployed on the ER-2 which simultaneously conducted the same racetrack flight patterns above the clouds. The straight legs of each oval were typically about 20 minutes in duration (~ 200 km) with the turns at each end making the horizontal extent of each oval roughly 250 km. The tangent points of upwind turns were set up in real time to be about 10 km downwind of a turret identified by the flight planning team at base from rapid-update GOES imagery. The July 31 flight targeted cirrus clouds streaming to the southeast from a convective complex that was visible from the operations base at Juan Santamaria airport near San Jose, Costa Rica. Remote sensing observations from both the DC-8 and the ER-2 suggest that the peak convective outflow was above the DC-8 ceiling, thus the in situ observations were in the lower part of the cirrus. Winds at flight level for this flight were surprisingly light and variable. On the August 5 and 8 flights the cirrus anvils extended westward from the convective cores selected. Winds at flight level for these two flights were much stronger and relatively steady. On these flights the DC-8 was unable to reach cloud tops but was able to get near to the top of the cirrus in later orbits. Seven complete orbits were flown on the July 31 flight and 5 complete orbits were flown on each of the August 5 and August 8 flights. It should be noted that during the August 8 flight the convective core feeding the initially selected cirrus anvil began to dissipate, so the pattern was moved to fly in a newly formed anvil nearby. It should also be noted that the DC-8 flew all of the orbits at the highest altitude possible at that point in the flight, increasing as the aircraft became lighter from fuel consumption as seen in VIII.2-4. This

provided an opportunity to sample each cloud at a range of temperatures, decreasing from nearly 245 K for early passes to about 220 K for the later passes for each flight.

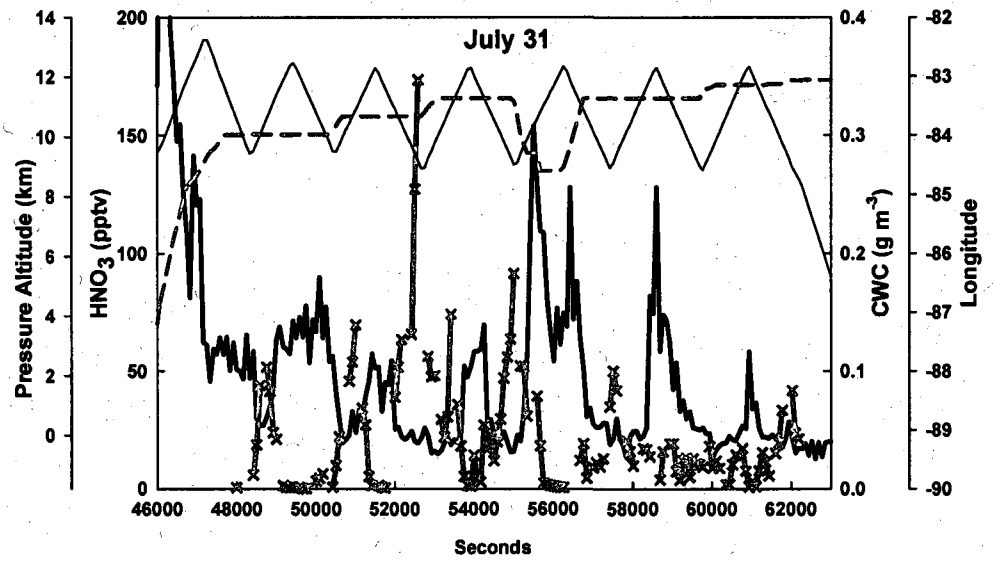

Figure VIII.2 Time Series of the July 31 Flight: HNO_3 (thick black), CWC (solid gray with hashes), pressure altitude (dashed gray) and longitude (thin black).

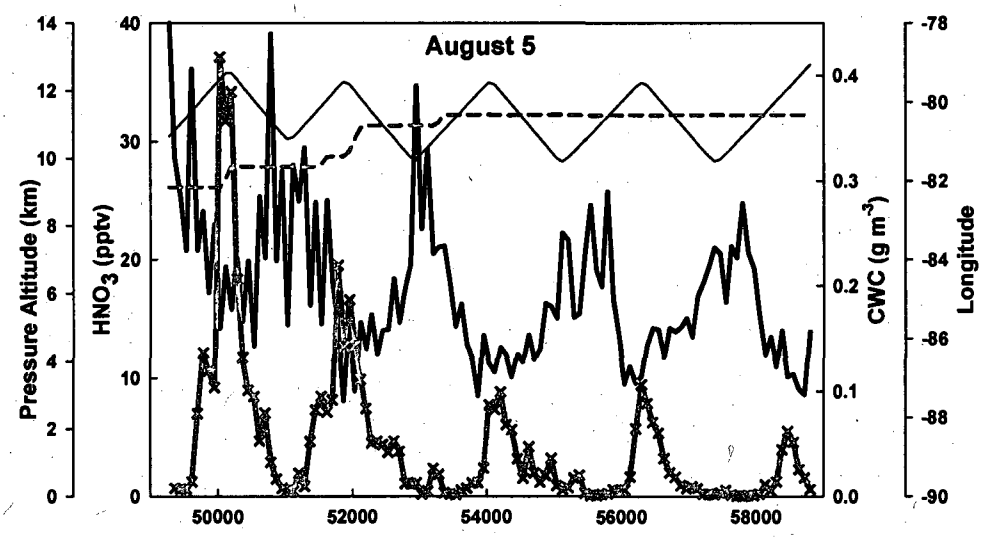

Figure VIII.3 Time Series of the August 5 Flight: HNO_3 (thick black), CWC (solid gray with hashes), pressure altitude (dashed gray) and longitude (thin black).

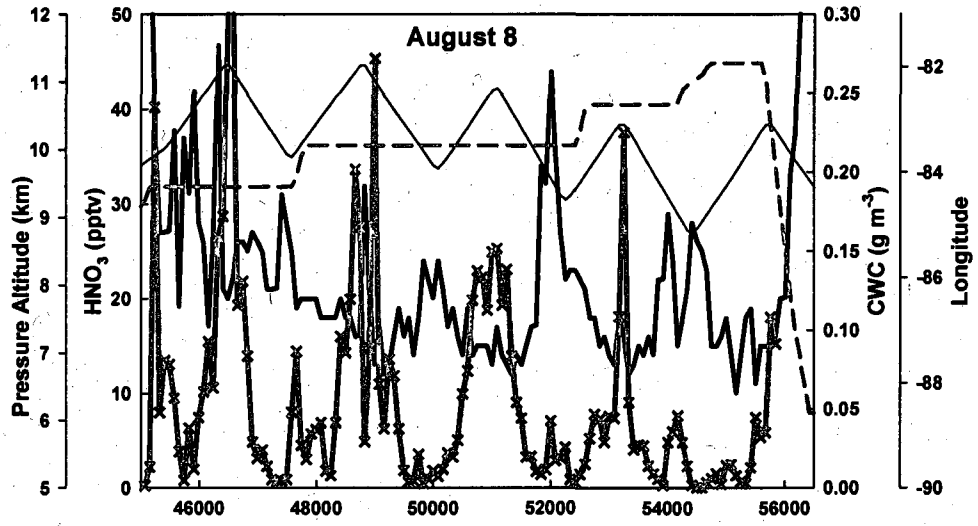

Figure VIII.4 Time Series of the August 8 Flight: HNO_3 (thick black), CWC (solid gray with hashes), pressure altitude (dashed gray) and longitude (thin black).

Presented are time series measurements made during the racetrack maneuvers of gas phase HNO_3 mixing ratios (solid black) and condensed water content (solid gray with hashes) averaged to HNO_3 instrument integration time on the July 31 flight (Figure VIII.2), the August 5 flight (Figure VIII.3) and the August 8 flight (Figure VIII.4). CWC data on the July 31 flight has discontinuities relative to HNO_3 that were ignored for plotting. Pressure altitude (dashed gray) and longitude (thin black) are shown for spatial reference.

During the cirrus cloud orbits on all three flights HNO_3 generally oscillated between about 5 to nearly 75 pptv with the exception of large enhancements around t=55,500-56,500 seconds and t=59,000 seconds during the July 31 flight (Figures VIII.2-4). The first large enhancement was observed on July 31 flight when the aircraft briefly descended below the visible cloud base (discussed in detail later) and the second was during the turn at the far south eastern end of an orbit where the cirrus was thin and

patchy (Figure VIII.2). In general, the lowest HNO_3 mixing ratios of each orbit were observed in the upwind end of each orbit and highest mixing ratios were at the downwind end. When orbits were repeated at constant altitude the variations of HNO_3 with position were quite similar in successive passes over the track. This is most clearly seen after t=53,000 seconds on the August 5 flight (Figure VIII.3). IWC mirrored this orbit-scale pattern in HNO_3, being highest at the upwind end near the convective core (where HNO_3 was lowest) and decreasing downwind (Figures VIII.2-4). Increases in IWC over shorter time intervals (smaller spatial scales) often coincided with decreased HNO_3 mixing ratios as well. This fine-scale anti-correlation is again most striking on the August 5 flight (Figure VIII.3).

CHAPTER IX

DISCUSSION

General Observations

Mixing ratios of HNO_3 were significantly depressed in cirrus clouds sampled during TC4 compared to the mean mixing ratio of 120 pptv for all out of cloud measurements in the same 9 - 12 km upper tropospheric altitude range. Two processes may contribute to the lower mixing ratios. First, some fraction of the air inside the clouds may represent convectively pumped air from the marine boundary layer where HNO_3 has been scavenged by precipitation [e.g. *Bertram et al.*, 2007], and second, cirrus ice crystals may have adsorbed HNO_3 in the UT surrounding the convective outflow. The striking anti-correlation with IWC (Figures VII.2-4) suggests that the latter process plays a non-negligible role. Likewise, the sharp increase in HNO_3 mixing ratios during the dip below the pilot defined visible cloud base on July 31 flight (Figure VII.2) appears to reflect a release of HNO_3 from evaporating cirrus ice crystals. Such release implies prior uptake of HNO_3, likely from UT air rather than detraining scavenged MBL air. The fact that the DC-8 was often below the altitude of peak outflow in cirrus that had fallen out of the thickest part of the anvil would imply that a significant fraction of the sampled air surrounding the ice crystals had not been recently convected. This could be more rigorously quantified using dilution factors derived from short-lived marine boundary layer (MBL) tracers detected in the UT, however, there were insufficient measurements

made in the MBL with which to compare to and constrain that estimate. Also, the observed increases of HNO_3 in thinner (downwind) regions of the cloud have to reflect contributions of upper tropospheric air since HNO_3 would not have been produced so quickly in detraining air depleted by scavenging [*Bertram et al.*, 2007]. We assume that the observed depletions of HNO_3 are primarily because of uptake onto the cirrus crystals as the anvil entrained UT air and/or the ice crystals settled into UT air below the altitude of maximum convective outflow.

Evidence for HNO_3 uptake onto cirrus ice particles

The premise that gas phase HNO_3 was depleted in cirrus clouds is based on comparisons to observations made in clear, dryer air at 9 - 12 km altitudes during TC4 and quantifying the magnitude of depletion remains subjective without measurements of condensed phase HNO_3. Mean mixing ratios of 60 pptv were observed in clear air during the three flights in the 30 minutes of UT sampling prior to and after the series of orbits on each flight. While 60 pptv is higher than in-cloud observations (consistently < 40 pptv on the last 5 orbits of the July 31 flight and all orbits on the August 5 and 8 flights) it is only half the mission mean (excluding transit flights to and from Costa Rica) of 120 pptv in the UT. It should be noted that the mission mean includes UT sampling in the subtropics, while the region near the racetracks on the three focus flights was clearly impacted by convection and cirrus processing. Based on this, we assume background mixing ratios of HNO_3 in the UT near Costa Rica into which deep convection was detraining were likely in the range of 60 - 120 pptv. In the following it is assumed that 100 pptv is a reasonable

estimate of UT HNO_3 before the cirrus formed. In-cirrus HNO_3 was observed at 5 - 75% of this assumed background, most often in the range 10 - 40%. As noted earlier, the depressed mixing ratios could be attributed to simple mixing of background UT air and convected marine boundary layer MBL with no HNO_3, but this would be difficult to reconcile with the observed anti-correlations with IWC and SAD. Alternatively, we postulate that uptake onto cirrus ice accounts for most of the observed depletion of HNO_3 and that the contribution of scavenged MBL was negligible at DC-8 flight levels. Contributions from mixing cannot be ruled out, but disregarding it provides constraint on the maximum uptake of HNO_3 onto the cirrus particles in the warm ITCZ clouds.

The inferred uptake onto cirrus ice is simply the 100 pptv background minus observed in-cloud HNO_3 mixing ratio, for each sample when IWC was detectable. The delta HNO_3 is converted to volumetric number density using in situ pressure and temperature and divided by mean observed SAD over each integration interval. Surface coverages of 0.01 to 0.67 $x10^{14}$ molecules$\cdot cm^{-2}$ are estimated, with substantial scatter (Figure IX.1). To examine temperature dependence, we estimate average surface coverages in 5 degree K temperature bins from ~219 K to ~243 K. Table IX.1 and Figure IX.1 suggest two-fold more uptake at the coldest temperature compared to the warmest, but the trend is not smooth or statistically significant. However, we note that the estimated coverages during TC4 are quite similar to those reported in *Zieris et al.* [2004] for temperatures of ~227 K and substantially smaller than all previous observations at temperatures below 220 K except for the anomalously low coverages reported by *Melinger et al.* [1999] at 196 K. The TC4 surface coverage estimates are plotted with the

temperature-bin-average HNO_3 molecular coverages from CRYSTAL-FACE reported in *Popp et al.* [2004] from ~198 K to ~218 K to show the full range of temperatures for which field observations have been reported (Figure IX.1). In addition, we use the non-dissociative Langmuir isotherm fit from the *Ullerstam et al.* [2005] laboratory experiments to predict surface molecular coverages at mean in situ temperatures for each TC4 sample,

$$\Theta = \Theta_{max} \times \frac{(K_{eq}P)^v}{1 + (K_{eq}P)^v}$$

where $v = 1$ (non-dissociative isotherm) and K_{eq} is the temperature dependant equilibrium constant from *Ullerstam et al.* [2004],

$$K_{eq} = -(5.1 \pm 0.4) \times 10^5 T + (12.3 \pm 0.9) \times 10^7$$

assuming Θ_{max} = 2.4 x 10^{14} molecules·cm^{-2} as found in the thin film studies. Vapor pressures of HNO_3 are based on a constant 100 pptv mixing ratio from the field based estimates, converted to partial pressure using the average temperature and pressure of each sample.

Table IX.1 HNO_3 Molecular Coverage on Cirrus Ice: Mean in-cloud ice surface area density and estimated mean HNO_3 molecular coverage during racetrack maneuvers from TC4 flights on July 31 and August 5 and 8.

Temperature Bin K	Mean Temperature K (Std.Dev.) *(range)*	Molecules · cm^{-2} x 10^{13} (Std.Dev) *(range)*	SAD $\mu m^2 \cdot cm^{-3}$ (Std.Dev.) *(range)*
219-224	223.1 (1.2) *(219.6-224.0)*	1.3 (0.9) *(0.3-4.2)*	3507 (2558) *(712-10677)*
224-229	225.5 (1.3) *(224.0-228.9)*	0.9 (0.5) *(0.3-2.5)*	3673 (2190) *785-10701*
229-234	230.1 (1.2) *(229.0-233.4)*	0.9 (0.8) *(0.1-3.7)*	6600 (6562) *412-32256*
234-239	235.8 (1.3) *(234.3-238.9)*	1.0 (1.2) *(0.1-6.7)*	6591 (5414) *415-23418*
239+	240.7 (1.1) *(239.3-242.8)*	0.7 (0.6) *(0.1-2.3)*	7267 (7998) *56-38344*

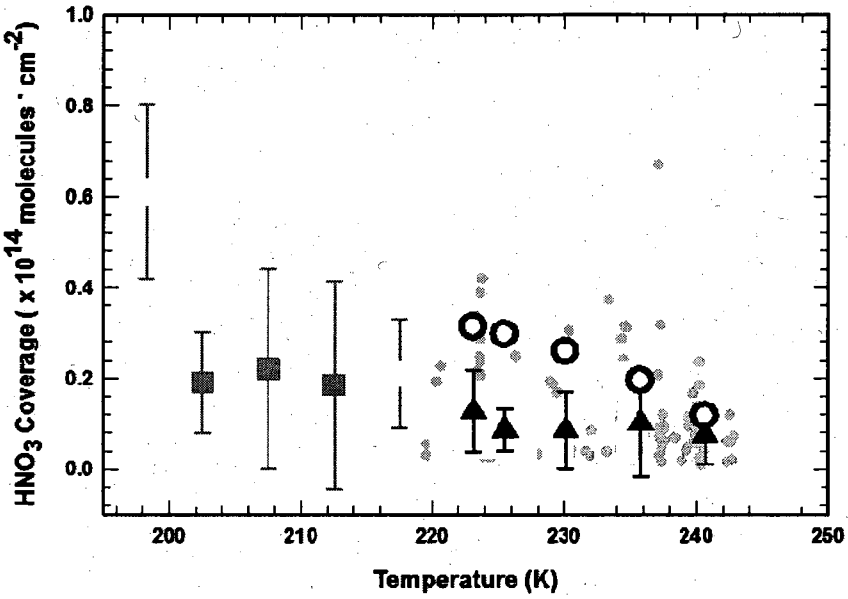

Figure IX.1 HNO_3 Molecular Coverage Versus Temperature. Solid circles represent discrete values calculated while in cirrus cloud during TC4 flights on July 31 and August 5 and 8 using SAD averaged to HNO_3 integration periods, measured HNO_3 mixing ratios and an assumed cirrus-free 100 pptv background HNO_3 mixing ratio. Triangles represent average TC4 coverages for 5° temperature bins ~219K to ~243K. Squares represent average coverages from *Popp et al.* [2004] figure 10 calculated for SADs greater than 200 $\mu m^2 \cdot cm^{-3}$ from data obtained during the CRYSTAL-FACE campaign. Error bars represent one standard deviation of averaged data in each temperature bin. Open circles represent predicted coverages from the Langmuir isotherm model presented in *Ullerstam et al.* [2005] using TC4 bin average temperatures and P_{HNO3} corresponding to 100 pptv.

Predicted coverages for the same 5 temperature bins are somewhat larger and show stronger temperature dependence than is apparent in the observations. At the warmest temperatures the means of the model based predictions and observations differ by less than the standard deviation of the observations, while below 235K predicted coverages are more than twice the observed means and barely fall within the upper limits defined by the distribution of the observations. The molecular coverages calculated here

are likely upper limits, because dilution by convected MBL air is neglected. *Ullerstam et al.* [2004] discussed both the scatter in observations from prior aircraft campaigns, and general disagreement with coverages estimated by extrapolating from equilibria determined in laboratory experiments. They suggest that in thick clouds (SAD ~ 10^4 $um^2 \cdot cm^{-3}$) equilibrium between ice and HNO_3 could be established in seconds to minutes, while in thin clouds (SAD ~ 10 $um^2 \cdot cm^{-3}$) the timescale would be on the order of hours. The SAD of cirrus sampled from the DC-8 during TC4 (Table IX.1) approached thick cloud levels, especially at warmer temperatures. While the lifetime of individual crystals is poorly constrained, it would seem that cloud lifetimes were long enough for equilibrium to be approached. *Ullerstam et al.* [2004] speculated that uptake of HNO_3 onto cirrus ice might be inhibited by surface impurities not present on ices grown in the laboratory. Observations during TC4 provide no insight into this possibility, since no composition data on the condensed phase is available. Key factors that likely contribute to the variability in the TC4 surface coverage estimates are first that the crystals had grown large enough to begin settling toward cloud base, with warmer temperatures and lower water vapor, and second that the mixing ratio of HNO_3 in air masses contacting the crystals probably was not constant as assumed. For example, cirrus ice crystals may have formed in air with very low HNO_3 in fresh outflow, then encountered progressively higher vapor pressure as the cloud spread and entrained UT air.

The estimated surface coverages during TC4 represent fractional coverages up to 28% of a saturated molecular monolayer (Θ) for an extreme case (based on 2.4 x 10^{14} $molecule \cdot cm^{-2}$ from *Ullerstam et al.*, [2005]), with the bin means (Table 1) only ranging

from 3 to 5 %. Clearly, uptake is far from saturated in these warm clouds, especially considering that our estimates are based on the assumption that all of the observed depletion of gas phase HNO_3 results from uptake by ice. Conversely, the depression of HNO_3 mixing ratios in the cirrus was substantial (on the order of 60 - 90%) and might have implications for chemistry in the UT if the removal was irreversible. However, the dip below cloud base during the July 31 flight suggests that vertical redistribution of HNO_3 by sedimenting cirrus ice may involve only modest displacements.

Vertical Redistribution of Nitric Acid by Cirrus

Sedimentation of cirrus ice crystals with adsorbed HNO_3 has been postulated as an efficient mechanism to remove HNO_3 from the upper troposphere [*Lawrence and Crutzen*, 1998]. This occurs when cirrus ice particles grow large enough for gravitational settling to remove them from the cirrus cloud. As ice particles settle out of the cloud into much dryer air below, they either melt and evaporate or sublime releasing adsorbed HNO_3 taken up in the cloud into the below cloud air. A key question is how far downward the particles carry the HNO_3 before release. As noted earlier, about halfway through the series of orbits during July 31 flight the DC-8 slowly descended to the cloud base (Figure VIII.2). Figure IX.2 is a detailed view of the time period during the drop below the cloud base.

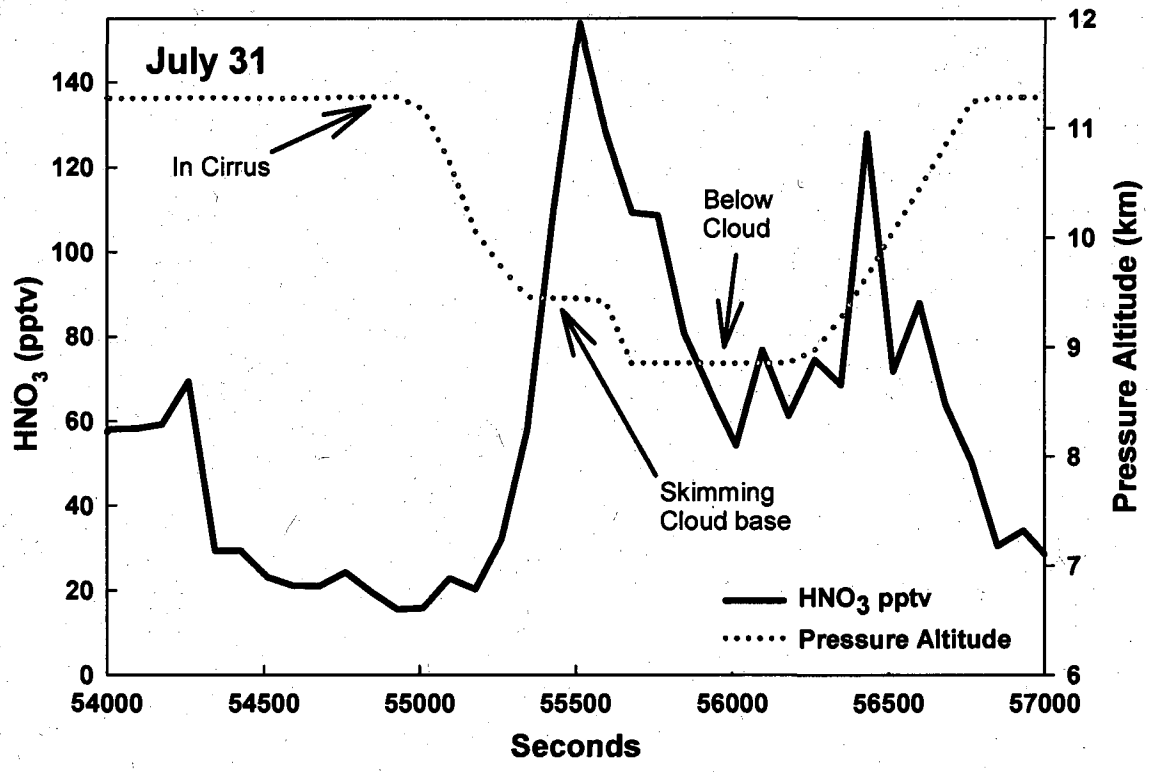

Figure IX.2 July 31 Flight Cirrus Dip Time Series: Time series plot from t=54000 seconds to t=57000 seconds on July 31 flight showing enhanced layer of gas phase HNO_3 just below the visible cloud base. HNO_3 mixing ratios decreased by a factor of 2 during the subsequent descent to ~0.5 km below the cloud base. The enhanced layer was also sampled during ascent into the clouds.

It can been seen that while skimming the cloud base, gas phase HNO_3 was observed to be enhanced by more than 120 pptv compared to the 20 pptv observed in thick cloud immediately preceding descent. After several minutes of level flight, the aircraft descended an additional 500 meters further below the cloud where HNO_3 decreased to about 60 pptv. The aircraft then began a slow ascent and the thin layer of enhanced HNO_3 was again observed at the cloud base. Vertical profiles of both ascent and descent are presented in Figure IX.3.

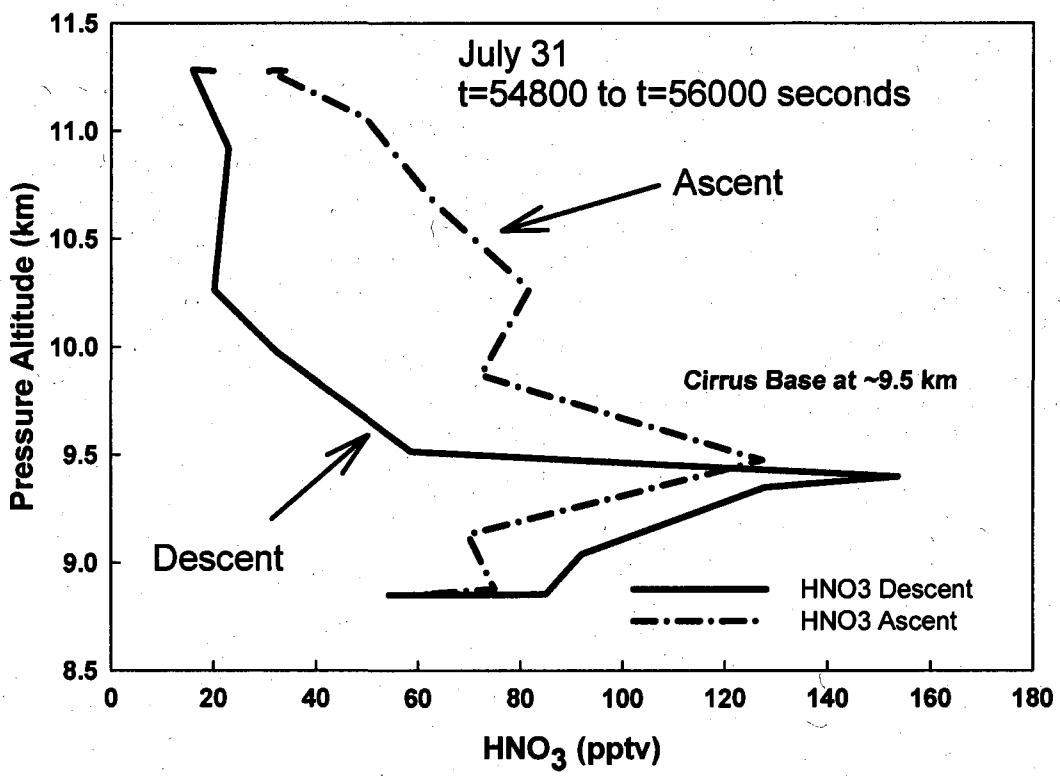

Figure IX.3 July 31 Flight Cirrus Dip Vertical Profile: Vertical profile of gas phase HNO_3 t=54800 seconds to t=56000. The enhanced layer can be clearly seen during both descent and ascent just below 9.5km, immediately below the visible base of the cirrus clouds.

These data are consistent with the hypothesized redistribution of HNO_3 by cirrus cloud particle sedimentation and subsequent evaporation as described in depth in *Lawrence and Crutzen* [1998]. However, the layer of enhancement observed here is remarkably thin and extremely close to the cloud base. Presumably, larger ice crystals like those observed in CRYSTAL-FACE would carry HNO_3 further below cloud base [*Popp et al.*, 2004] but vertical redistribution by the cirrus clouds sampled from the DC-8 in TC4 appears limited to the thickness of the cirrus shield.

CHAPTER X

CONCLUSION

Gas phase HNO_3, IWC, and SAD observations in warm cirrus clouds (~219K-243K) during three focused and repeated encounters in the tropical upper troposphere near Costa Rica during the NASA TC4 field campaign in 2007 are presented. In-cloud depletions of HNO_3 were observed and appear positively correlated to increasing water content and ice surface area density. Based on observations from the same study, we assume that the out-of-cloud HNO_3 background mixing ratio is approximately 100 pptv and the difference in observations made while in-cloud represent HNO_3 adsorbed onto ice particles. With these assumptions, average molecular coverages of HNO_3 on ice particles ranged from 0.7×10^{13} to 1.3×10^{13} molecules·cm^{-2} for 5 different temperature bins. This is somewhat lower than, but within a factor of 5 of, laboratory measurements summarized in *Ullerstam et al.* [2005] where molecular coverages on ice at 229K for $P(HNO_3)$/hPa from 3.0×10^{-8} to 6.3×10^{-8} (40-83 pptv) ranged from 3.8×10^{13} to 7.9×10^{13} molecules·cm^{-2}. Our observations suggest the cirrus ice was highly under-saturated with respect to HNO_3 and represents fractional coverages of HNO_3 on ice (Θ / Θ_{max}) of about 0.01 to 0.04 (assuming $\Theta_{max} = 2.4 \times 10^{14}$ molecules · cm^{-2}). However, this was enough to affect near total depletion of gas phase HNO_3 at periods of high IWC and SAD. Although there is no obvious temperature dependence seen in our molecular surface coverage on ice, our observations appear to be less than

those presented in *Popp et al.* [2004] from measurements made during CRYSTAL-FACE in slightly cooler tropical upper tropospheric cirrus cloud. This supports prior laboratory work suggesting a negative temperature dependence on uptake. Evidence of gravitational settling and subsequent evaporation of cirrus ice particles releasing HNO_3 back to the gas phase was observed during the July 31 flight; however the magnitude of this single event is not sufficient to support large scale redistribution of HNO_3 similar to that described in *Lawrence and Crutzen* [1998]. Further investigations into the magnitude of the redistributive capabilities of cirrus clouds would benefit from repeated vertical profiles in and beneath such formations and would ideally include direct in situ measurements of both gas and condensed phase HNO_3.

PART 3. SUMMARY OVERVIEW

NSF and NASA have played a critical role in the advancement of our understanding of the Earth's climate and atmospheric chemistry. Whether it is Arctic haze or the impact of cirrus clouds on ozone production, in situ aircraft measurements are an important part of developing the complex models necessary to accurately gauge the health of the atmosphere. Also, as remote sensing instruments aboard satellites become more prevalent, high sensitivity airborne measurements continue to be necessary to accurately calibrate and validate them. In this thesis, some findings from two different major aircraft campaigns are reported.

During TOPSE, the seasonal evolution of fine aerosol sulfate in the Arctic troposphere was observed to be consistent with the phenomenon of Arctic haze. Arctic haze has been attributed to pollution from sources in the Arctic and pollution transported meridionally along stable isentropes into the Arctic in geographically broad but vertically narrow bands. These layers became more prevalent at higher altitudes, as the season progressed toward summer and the relevant isentropes are not held so close to the surface. As the season progressed, elevated mixing ratios, and higher variability was observed at progressively higher altitudes. In May, mixing ratios at the lowest altitudes declined, but still remained higher than in February at all altitudes. The high variability in our measurements likely reflects the vertical heterogeneity of the wintertime Arctic atmosphere as the airborne sampling platform passed in and out of these layers. It is

presumed that mixing ratios and variability will continue to decline at all altitudes into the summer as wet deposition processes become important in removing aerosol $SO_4^=$ from the troposphere.

In 2007, the impacts of cirrus clouds on climate and the composition of the tropical upper troposphere were studied during TC4. One chemical impact that has been postulated is removal and vertical redistribution of HNO_3 through uptake on cirrus particles. Limited previous sampling campaigns have provided somewhat differing results and are not fully compatible with theory developed from laboratory studies. During the field campaign the NASA DC-8 research aircraft spent approximately 41 flight hours in the tropical upper troposphere. Close to half of the sampling time in the upper troposphere consisted of orbiting "racetrack" patterns in cirrus clouds from anvil outflow. On several flights, the same cloud region was traversed multiple times, revealing persistent regions of "thicker" cloud with less gas phase HNO_3 and contrasting "thinner" cloud with relatively enhanced gas phase HNO_3. We speculate that the difference is due primarily to adsorption of HNO_3 onto cirrus ice surfaces. Strong enhancements of HNO_3 at the base of a cirrus anvil suggest vertical redistribution of HNO_3 by sedimenting cirrus particles and subsequent particle sublimation and HNO_3 evaporation. The impact of released HNO_3, however, appeared to be restricted to a very thin layer just below the cloud.

LIST OF REFERENCES

Abbatt, J. P. D. (1997), Interaction of HNO_3 with water-ice surfaces at temperatures of the free troposphere, *Geophys. Res. Lett.*, *24*(12), 1479-1482.

Arora, O. P., D. J. Cziczo, A. M Morgan, J. P. D. Abbott, R. F. Niedziela (1999), Uptake of nitric acid by sub-micron-sized ice particles, *Geophys. Res. Lett.*, *26*(24), 3621-3624.

Atlas, E. L., B. A. Ridley, and C. A. Cantrell (2003), The Tropospheric Ozone Production about the Spring Equinox (TOPSE) Experiment: Introduction, *J. Geophys. Res.*, 108(D4), 8353, doi:10.1029/2002JD003172

Barrie, L. A. (1985), Atmospheric Particles: Their physical and chemical characteristics, and deposition processes relevant to the chemical composition of glaciers, *Annals of Glaciology, 7*, 100-108.

Barrie, L.A. and R.M. Hoff (1985), Five years of air chemistry observation in the Canadian Arctic, *Atmos. Environ., 19*, 1995-2010.

Barrie, L.A. (1986), Arctic air pollution: An overview of current knowledge, *Atmos. Environ., 20*, 643-663, 1986.

Bertram, T. H., et al. (2007), Direct measurements of the convective recycling of the upper troposphere, *Science*, 315(5813), 816-820, doi: 10.1126/science.1134548.

Blanchet, J. and R. List (1983), Estimation of optical properties of arctic haze using a Numerical model, *Atmosphere-Ocean, 21*, 444-465.

Blanchet, J. (1989), Toward estimation of climatic effects due to arctic aerosols, *Atmos. Environ.*, 23, 2609-2625.

Bradley, R. S., F.T. Keimig, H.F. Diaz (1992), Climatology of surface-based inversions in the North American Arctic, *J. Geophys. Res.*, 97, 15,699-15,712.

Brock, C.A., L.F. Radke, J.H. Lyons, and P.V. Hobbs (1989), Arctic hazes in summer Over Greenland and the North American Arctic. I: Incidence and origins, *J. Atmos. Chem., 9*, 129-148.

Brock, C.A., L.F. Radke, and P.V. Hobbs (1990), Sulfur in particles in arctic hazes derived from airborne in situ and lidar measurements, *J. Geophys. Res., 95*, 22,369-22,387.

Cofer, W.R., and R.A. Edahl (1985), A new technique for collection, concentration and determination of gaseous tropospheric formaldehyde, *Atmos. Environ.*, 20, 979-984.

Cofer, W.R., V.G. Collins, and R.W. Talbot (1986), Improved aqueous scrubber for collection of soluble atmospheric trace gases, *Environ. Sci. Technol.*, 19, 557-560.

Dibb, J. E., R. W. Talbot, G. Seid, C. Jordan, E. Scheuer, E. Atlas, N. J. Blake, and D. R. Blake (2002), Airborne sampling of aerosol particles: Comparison between surface sampling at Christmas Island and P-3 sampling during PEM-Tropics B, *J. Geophys. Res.*, 107, 8230, doi:10.1029/2001JD000408.

Dibb, J. E., R. W. Talbot, E. Scheuer, G. Seid, L. DeBell, B. Lefer, and B. Ridley (2003), Stratospheric influence on the northern North American free troposphere during TOPSE: ^{7}Be as a stratospheric tracer, *J. Geophys. Res.*, 108(D4), 8363, doi:10.1029/2001JD001347.

Dibb, J. E., M. Arsenault, M. C. Peterson, and R. E. Honrath (2002), Fast nitrogen oxide photochemistry in Summit, Greenland snow, *Atmos. Environ.*, 36, 2501-2511.

Hinds, W.C. Acceleration and curvilinear particle motion, *Aerosol Technology*, pp. 105-110, John Wiley & Sons, Inc., New York, 1982.

Hudson, P. K., J.E. Shilling, M. A. Tolbert, O. B. Toon (2002), Uptake of nitric acid on ice at tropospheric temperatures: Implications for cirrus clouds, *J. Phys. Chem. A*, *106*, 9874-9882.

Hynes, R. G. M. A. Fernandez, R. A. Cox (2002), Uptake of HNO_3 on water-ice and coadsorption of HNO_3 and HCl in the temperature range 210-235 K, *J. Geophys. Res.*, *107*(D24), 11, doi:10.1029/2001JD001557.

Jacob, D. J., et al. (1996), Origin of ozone and NO_x in the tropical troposphere: A photochemical analysis of aircraft observations over the South Atlantic basin, *J. Geophys. Res.*, *101*(D19), 24235-24250.

Kahl, J.D. (1990), Characteristics of the low-level temperature inversion along the Alaskan Arctic coast, *Int. J. Climatol.*, 10, 537-548.

Kahl, J.D., M.C. Serreze, and R.C. Schnell (1992), Tropospheric low-level temperature inversions in the Canadian Arctic, *Atmosphere-Ocean, 30*, 511-529.

Keene, W.C., A.P.P Pszenny, J.N. Galloway, and M.E. Hawley (1986), Sea-salt Corrections and interpretations of constituent ratios in marine precipitation, *J. Geophys. Res.*, 6647-6658.

Keene, W.C., J.R. Maben, A.P.P Pszenny, and J.N. Galloway (1993), Measurement technique for inorganic chlorine gases in the marine boundary layer, *Environ. Sci. and Tech.*, 27.

Klemm, O., and R.W. Talbot (1991), A sensitive method for measuring atmospheric concentrations of sulfur dioxide, *J. Atmos. Chem.*,13, 325-342.

Klonecki, A., P. Hess, L. Emmons, L. Smith, J. Orlando, and D. Blake (2003), Seasonal changes in the transport of pollutants into the Arctic troposphere-model study, *J. Geophys. Res.*, 108(D4), 8367, doi:10.1029/2002JD002199.

Kondo, Y., et al. (2003), Uptake of reactive nitrogen on cirrus cloud particles in the upper troposphere and lowermost stratosphere, *Geophys. Res. Lett.*, *30*(4), 1154, doi:10.1029/2002GL015549.

Lawrence, M. G., and P. J. Crutzen (1998), The impact of cloud particle gravitational settling on soluble trace gas distributions, *Tellus Ser.B*, *50*, 263-289.

Lazrus, A.L., and R.J. Ferek (1984), Acidic sulfate particles in the winter arctic atmosphere, *Geophys. Res. Lett.*, 11, 417-419.

Meier, A., and J. Hendricks (2002), Model studies on the sensitivity of upper tropospheric chemistry to heterogeneous uptake of HNO_3 on cirrus ice particles, *J. Geophys. Res.*, *107*(D23), 4696, doi:10.1029/2001JD000735.

Meilinger, S. K., et al. (1999), HNO_3 partitioning in cirrus clouds, *Geophys. Res. Lett.*, *26*(14), 2207-2210.

Neuman, J. A., et al. (2001), In situ measurements of HNO_3, NO_y, NO, and O_3 in the lower stratosphere and upper troposphere, *Atmos. Environ*, *35*(33), 5789-5797.

Popp, P. J., et al. (2004), Nitric acid uptake on subtropical cirrus cloud particles, *J. Geophys. Res.*, *109*, D06302, doi:10.1029/2003JD004255.

Radke, F.L., and P.V. Hobbs (1984), Airborne observations of arctic aerosols. III: Origins and effects of airmasses, *Geophys. Res. Lett.*, 11, 401-404.

Radke, F.L., J.H. Lyons, D.A. Hegg, P.V. Hobbs, and I.H. Bailey (1984), Airborne Observations of arctic aerosols. I: Characteristics of arctic haze, *Geophys. Res. Lett.*,, *11*, 393-396.

Rahn, K.A. and R.J. McCaffrey (1979), Long-range transport of pollution aerosol to the Arctic: A problem without boarders, paper presented at the WMO Symp. On the Long Range Transport of Pollutants and its Relation the General Circulation Including Stratospheric/Tropospheric Exchange Processes, pp. 25-35, Sofia, 1-5 October 1979. WMO No. 538.

Rahn, K.A. and N.Z. Heidman, Progress in Arctic air chemistry, 1977-1980: a comparison of the first and second symposia, *Atmos. Environ.*, 15, 1345-1348

Ridley B., E. Atlas, D. Montzka, E. Browell, C. Cantrell, D. Blake, N. Blake, M. Coffey, R. Cohen, R. DeYoung, J. Dibb, F. Eisele, F. Flocke, A. Fried, F. Grahek, W. Grant, J. Hair, J. Hannigan, B. Heikes, B. Lefer, L. Mauldin, R. Shetter, J. Snow, R. Talbot, J. Thornton, J. Walega, A. Weinheimer, (2003), Ozone depletion events observed in the high latitude surface layer during the TOPSE aircraft program, *J. Geophys. Res.*, 108(D4), 8356, doi:10.1029/2001JD001507.

Schmitt, C. G., and A. J. Heymsfield (2005), Total surface area estimates for individual ice particles and particle populations, *J. App. Meteorol.*, *44*(4), 467-474.

Shaw, G.E., and M.A.K. Khalil (1989), Arctic haze, *The handbook of environmental chemistry*, vol. 4, edited by O. Hutzinger, pp. 89-91, Springer-Verlag, Berlin Heidelberg.

Staudt, A. C., D. J. Jacob, F. Ravetta, J. A. Logan, D. Bachiochi, T. N. Krishnamurti, S. Sandholm, B. Ridley, H. B. Singh, B. Talbot (2003), Sources and chemistry of nitrogen oxides over the tropical Pacific, *J. Geophys. Res.*, *108*(D2), 8239, doi10.1029/2002JD002139.

Tabazadeh, A., O. B. Toon, E. J. Jensen, (1999), A surface chemistry model for nonreactive trace gas adsorption on ice: Implications for nitric acid scavenging by cirrus, *Geophys. Res. Lett.*, *26*(14), 2211-2214.

Talbot, R.W., K.M. Beecher, R.C. Harriss, and W.R. Cofer (1988), Atmospheric geochemistry of formic and acetic acids at a mid-latitude temperate site, *J. Geophys. Res.*, 1638-1652.

Talbot, R.W., A.S. Vijgen, and R.C. Harriss (1990), Measuring tropospheric HNO_3: problems and prospects for nylon filter and mist chamber techniques, *J. Geophys. Res.*, 7553-7561, 1990.

Talbot, R.W., A.S. Vijgen, R.C. Harriss (1992), Soluble Species in the arctic summer troposphere: acidic gases, aerosols, and precipitation, *J. Geophys. Res., 97*, 16,531-16,543.

Talbot, R.W., J.E. Dibb, E.M. Scheuer, Y. Kondo, M. Koike, H.B. Singh, L.B. Salas, Y. Fukui, J.O. Ballenthin, R.F. Meads, T.M. Miller, D.E. Hunton, A.A. Viggiano, D.R. Blake, N.J. Blake, E. Atlas, F. Flocke, D.J. Jacob, and L. Jaegle (1999), Reactive nitrogen budget during the SONEX mission, *Geophys. Res. Lett.*, 20, 3057-3060.

Thakur, A. N., H. B. Singh, P. Mariani, Y. Chen, Y. Wang, D. J. Jacob, G. Brasseur, J. F. Muller, M. Lawrence (1999), Distribution of reactive nitrogen species in the remote free troposphere: data and model comparisons, *Atmos. Environ.*, *33*(9), 1403-1422.

Twohy, C. H., A. J. Schanot, W. A. Cooper (1997), Measurement of condensed water content in liquid and ice clouds using an airborne counterflow virtual impactor, *J. Atmos. Oceanic Technol., 14*(1), 197-202.

Ullerstam, M. T. Thornberry, J. P. D. Abbatt (2005), Uptake of gas-phase nitric acid to ice at low partial pressures: evidence for unsaturated surface coverage, *Faraday Discuss, 130*, 211-226.

Warneck, P. (1988), Sulfur compounds in the atmosphere, in *Chemistry of the Natural Atmosphere*, vol. 41, pp. 484-5423, Academic Press, California.

Weinheimer, A. J., T. L. Campos, J. G. Walega, F. E. Grahek, B. A. Ridley, D. Baumgardner, C. H. Twohy, B. Gandrud, E. J. Jensen (1998), Uptake of NO_y on wave-cloud ice particles, *Geophys. Res. Lett.*, *25*(10), 1725-1728.

Ziereis, H., et al. (2004), Uptake of reactive nitrogen on cirrus cloud particles during INCA, *Geophys. Res. Lett.*, *31*, L05115, doi:10.1029/2003GL018794.

Zondlo, M. A. S. B. Barone, M. A. Tolbert (1997), Uptake of HNO_3 on ice under upper tropospheric conditions, *Geophys. Res. Lett.*, *24*(11), 1391-1394.